arXiv:1601.01701v2 [astro-ph.CO] 2 May 2016

A 6% measurement of the Hubble parameter at $z \sim 0.45$: direct evidence of the epoch of cosmic re-acceleration

Michele Moresco,[1,2] **Lucia Pozzetti,**[2] **Andrea Cimatti,**[1] **Raul Jimenez,**[3,4,5,6] **Claudia Maraston,**[7] **Licia Verde,**[3,4,5,9] **Daniel Thomas,**[7] **Annalisa Citro,**[1,2] **Rita Tojeiro,**[8] **and David Wilkinson**[7]

[1]Dipartimento di Fisica e Astronomia, Università di Bologna, V.le Berti Pichat, 6/2, 40127, Bologna, Italy

[2]INAF - Osservatorio Astronomico di Bologna, via Ranzani 1, 40127 Bologna, Italy

[3]ICREA & ICC, University of Barcelona (IEEC-UB), Barcelona 08028, Spain

[4]Radcliffe Institute for Advanced Study, Harvard University, MA 02138, USA

[5]Institute for Theory & Computation, Harvard University, 60 Garden Street, Cambridge, MA 02138

[6]Institute for Applied Computational Science, Harvard University, MA 02138, USA

[7]Institute of Cosmology and Gravitation, Dennis Sciama Building, University of Portsmouth, Burnaby Road, Portsmouth, PO1 3FX, UK

[8]School of Physics & Astronomy, University of St Andrews, KY16 9SS, UK

[9]Institute of Theoretical Astrophysics, University of Oslo, 0315 Oslo, Norway

E-mail: michele.moresco@unibo.it, lucia.pozzetti@oabo.inaf.it, a.cimatti@unibo.it, rauljimenez@g.harvard.edu, claudia.maraston@port.ac.uk, liciaverde@icc.ub.edu, daniel.thomas@port.ac.uk, annalisa.citro@unibo.it, rmftr@st-andrews.ac.uk, david.wilkinson@port.ac.uk

Abstract. Deriving the expansion history of the Universe is a major goal of modern cosmology. To date, the most accurate measurements have been obtained with Type Ia Supernovae (SNe) and Baryon Acoustic Oscillations (BAO), providing evidence for the existence of a transition epoch at which the expansion rate changes from decelerated to accelerated. However, these results have been obtained within the framework of specific cosmological models that must be implicitly or explicitly assumed in the measurement. It is therefore crucial to obtain measurements of the accelerated expansion of the Universe independently of assumptions on cosmological models. Here we exploit the unprecedented statistics provided by the Baryon Oscillation Spectroscopic Survey (BOSS, [1, 2, 3]) Data Release 9 to provide new constraints on the Hubble parameter $H(z)$ using the *cosmic chronometers* approach. We extract a sample of more than 130000 of the most massive and passively evolving galaxies, obtaining five new cosmology-independent $H(z)$ measurements in the redshift range $0.3 < z < 0.5$, with an accuracy of $\sim$11–16% incorporating both statistical and systematic errors. Once combined, these measurements yield a 6% accuracy constraint of $H(z = 0.4293) = 91.8 \pm 5.3$ km/s/Mpc. The new data are crucial to provide the first cosmology-independent determination of the transition redshift at high statistical significance, measuring $z_t = 0.4 \pm 0.1$, and to significantly disfavor the null hypothesis of no transition between decelerated and accelerated expansion at 99.9% confidence level. This analysis highlights the wide potential of the cosmic chronometers approach: it permits to derive constraints on the expansion history of the Universe with results competitive with standard probes, and most importantly, being the estimates independent of the cosmological model, it can constrain cosmologies beyond – and including – the ΛCDM model.

Contents

1 Introduction

Almost 15 years have now passed since the discovery of the accelerated expansion of the Universe, based on the work by refs. [4] and [5]. Since then, constraining the expansion rate of the Universe as a function of redshift $H(z)$ has become one of the most compelling tasks of modern cosmology, since it determines the scale factor $a(t)$ in the Friedmann-Lemaitre-Robertson-Walker (FLRW) metric; as a consequence, this allows us to probe the properties of the fundamental components of the Universe, helping to better understand their nature. Widening the panorama of cosmological probes is therefore of extreme interest, in order to take advantage of the strength of each method and to keep systematics under control (for a detailed review, see ref. [6]).

So far, the best measurements have been obtained with standard candles (SNe) [4, 5] and standard rulers (BAO) [7, 8]. These cosmological probes have provided exceptional results over the last decades, and contributed, together with the study of the Cosmic Microwave Background (CMB) [9], to the development of the standard ΛCDM cosmological model. One of their main limitations, however, is that they do not constrain the Hubble parameter directly, but one of its integrals (e.g., the luminosity distance [4]) or the parameters that are used to model it. In order to set constraints on the cosmological model, it is necessary to obtain an independent determination of the expansion rate, which could then be used to test the model itself.

A possible way to achieve this task is given by the "cosmic chronometers" method. According to this method, firstly suggested by ref. [10], the relative age of old and passive galaxies dz/dt can be used to directly constrain the expansion history of the Universe. The most important point to emphasize is that because the differential dating of passively evolving galaxies only depends on atomic physics and does not include any integrated distance

measurement over redshift, it is independent of the cosmological model or assumptions about the metric, and thus can be used to place constraints on it.

In ref. [11], analyzing a sample of ∼11000 massive and passive galaxies, eight new measurements of the Hubble parameter have been provided with an accuracy of ∼5-12% in the redshift range $0.15 < z < 1.1$, significantly extending the redshift coverage and precision of previous similar analysis [12, 13]. The majority of the sample in this work was at low redshift ($z < 0.3$), where the most accurate constraints were obtained. The potential of this new method in comparison with more standard probes has been studied by many authors [14, 15, 16, 17], which demonstrated how the cosmic chronometers method can be competitive for many aspects with Supernovae type Ia (SNe) and Baryon Acoustic Oscillation (BAO) in constraining cosmological parameters.

In this paper, we want to exploit the phenomenal set of data provided by the SDSS-III Baryon Oscillation Spectroscopic Survey (BOSS, [1, 2, 3]), which represents the largest sample of massive galaxies spectra available so far at $0.2 < z < 0.8$, to provide new $H(z)$ measurements with the highest possible accuracy at these redshifts. This sample allows us to minimize all possible uncertainties, by improving the statistics used so far by ∼2 orders of magnitude at these redshifts. BOSS data also represent a very well defined spectroscopic sample, being targeted to select the most massive envelope of the galaxy population at these redshifts [18]. Moreover, the redshift range probed by BOSS proves to be fundamental to set cosmology independent constraints on the redshift at which the Universe expansion turns from decelerated to accelerated, which we refer to as the cosmological transition redshift [19, 20, 21, 22].

This paper is organized as follows. In section 2 we introduce the technique, its potential drawbacks and how they are addressed. In section 3 we describe how the dataset has been selected and describe its properties. In section 4 we provide the stellar metallicity constraints for our sample. We also discuss how the relation between parameters and observables used in the method has been obtained and calibrated. Finally, in section 5 we present our results, providing five new $H(z)$ points in the redshift range $0.35 < z < 0.5$, and using them, in combination with available literature data, to obtain new constraints on the cosmological transition redshift.

2 Method: the cosmic chronometers approach

An accurate measurement of the expansion rate as a function of cosmic time is extremely challenging. An alternative and promising method is the "cosmic chronometers" approach, which uses the fact that the expansion rate can be expressed as $H(z) = \dot{a}/a = -1/(1+z)\,dz/dt$. Since the quantity dz is obtained from spectroscopic surveys with high accuracy, the only quantity to be measured is the differential age evolution of the Universe (dt) in a given redshift interval (dz). Therefore, a measurement of dt corresponds to a direct cosmology-independent measurement of the Hubble parameter. There are two main challenges to be faced: the identification of an optimal tracer of the aging of the Universe with redshift (a "cosmic chronometer"), and the reliable dating of its age.

The best cosmic chronometers are galaxies that are evolving passively on a timescale much longer than their age difference. Based on several observational results, there is general agreement that these are massive ($\mathcal{M}_{\rm stars} > 10^{11}\mathcal{M}_{\odot}$) early-type galaxies which formed the vast majority (>90%) of their stellar mass rapidly (∼0.1-0.3 Gyr) early in the Universe (at high-redshifts $z > 2-3$), and have not experienced any subsequent major episode of star for-

mation since. Therefore they are the oldest objects at any redshift [23, 24, 25, 26, 27, 28, 29]. Thus, when observed at cosmic times considerably later than their formation epoch, the age evolution of their stars serves a clock that is synchronized with the evolution of cosmic time. Previous works [11, 30, 31, 32] have also demonstrated that it is possible to obtain reliable and accurate cosmic chronometers using passively evolving selected galaxies. Recently, the independent analysis of SDSS-DR8 luminous red galaxies by ref. [33] has confirmed that massive and quiescent galaxies can be reliably used as cosmic chronometers.

It is important to underline that the main strength of this method is that it relies on a *differential approach*. On the one hand, it should be noted that the relevant quantities in this approach are the relative ages dt, which have the advantage of factorizing out systematic effects inherent to absolute age estimates. On the other hand, this method allows us to keep under control many observational biases which may affects this analysis. One of the main issues is the so-called progenitor bias [34, 35], for which high-redshift ETGs are biased by sampling only the oldest and more massive progenitors of more local galaxies, therefore changing the slope of the age-redshift relation. This effect is more severe when galaxy samples are compared in wide redshift ranges, but here each $H(z)$ value is estimated within small redshift slices, with $\Delta z = 0.1$ (as discussed in section 5.1) corresponding to a difference in cosmic time of approximatively 0.7 Gyr at $z \sim 0.45$. This is a rather short time for a potential significant evolution of these massive and passive systems, in particular considering that on average they would require more than the age of the Universe to double their mass [27, 36]. Moreover, the progenitor bias dominates the low-mass range of the distribution, whereas BOSS galaxies have been selected to be the most massive galaxies ($\log(\mathrm{M}/\mathrm{M}_{\odot}) \gtrsim 11$) between $0.3 < z < 0.7$ (see Fig. 1 of ref. [18]), and further divided in bin of velocity dispersion, which is a proxy for stellar mass.

To minimize the dependence of the age estimate on evolutionary stellar population synthesis (EPS) models, refs. [11, 32] proposed an improvement to this technique, consisting in studying a direct observable of galaxy spectra, the 4000 Å break ($D4000$), instead of galaxy ages. The $D4000$ feature is a break in the observed spectrum of galaxies defined as the ratio between the continuum flux densities $\langle F_{\nu} \rangle$ in a red band and a blue band around 4000 Å restframe [37]. The break originates from the onset of a series of metal absorption features, and is known to correlate with the stellar metallicity and age of the stellar population [38], and to be less dependent on the star formation history (SFH) for old stellar populations. Different choices have been proposed to measure the $D4000$, changing the range of the red and blue bands [37, 38, 39]. In this work, we considered the definition with narrower bands (D_n4000, 3850–3950 Å and 4000–4100 Å), since it has been shown to be less affected by potential reddening effects [39]. The assumption of a linear relation between $D4000$ and age of a galaxy has been proven to be an extremely good approximation for various $D4000$ ranges (see refs. [11, 32]), i.e.

$$D_n4000 = A(SFH, Z/Z_{\odot}) \cdot \mathrm{age} + B, \tag{2.1}$$

where $A(SFH, Z/Z_{\odot})$ is the slope of the D_n4000–age relation, and B its normalization. From eq. 2.1, it is therefore possible to express the Hubble parameter as:

$$H(z) = -\frac{1}{1+z} A(SFH, Z/Z_{\odot}) \frac{dz}{dD_n4000}, \tag{2.2}$$

where now statistical and systematic effects have been decoupled. The factor dz/dD_n4000 is only dependent on observables, while degeneracies between parameters or assumptions of EPS models are contained in the factor $A(SFH, Z/Z_{\odot})$. The main source of systematic errors

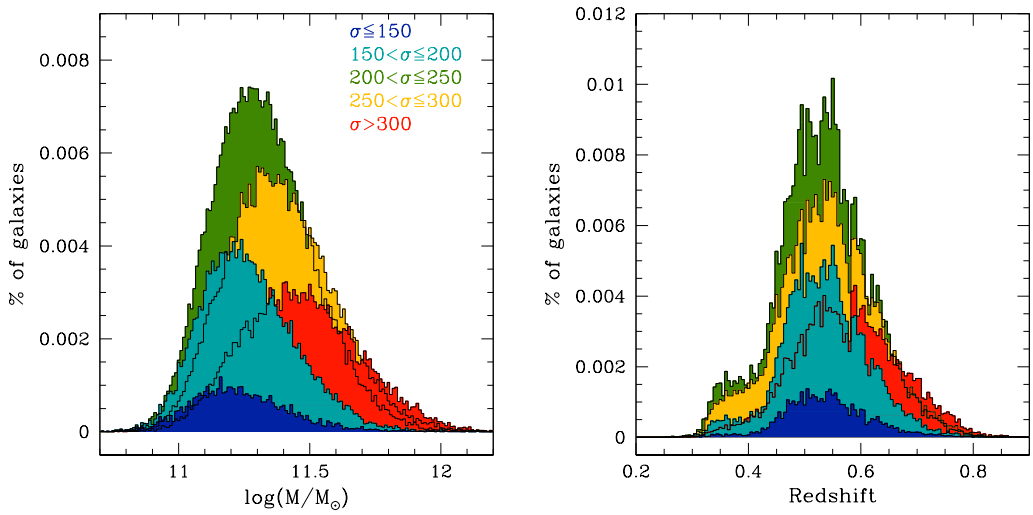

Figure 1. Stellar mass (left panel) and redshift (right panel) distributions, colored by the various velocity dispersion subsamples.

is the adopted EPS model that quantifies the dependence of the D_n4000 on age, metallicity Z and SFH. In Sect. 4.2 we will discuss the robustness of the assumption in Eq. 2.1, as well as the detailed dependence of the factor $A(SFH, Z/Z_{\odot})$ on metallicity and SFH.

In ref. [11] it was demonstrated that this new approach, which relies on the spectroscopic differential evolution of cosmic chronometers, is extremely robust against the choice of EPS models, and does not strongly depend on the SFH assumptions, the reason being that the selection criteria adopted significantly reduce the possibility of having prolonged SFHs, and spectra are usually well-fit with models with short star formation bursts.

3 Data and sample selection

The BOSS survey was designed to accurately map the clustering of large-scale structures up to $z \sim 0.7$, and in particular to measure the baryonic acoustic oscillation scale and constrain the expansion history of the Universe. It collected both photometric and spectroscopic data for ∼1.5 million galaxies over approximatively 10000 square degrees. The sample comprises the standard *ugriz* SDSS photometry; the spectroscopic sample has been photometrically targeted with a color cut in the $(g-r)$-$(r-i)$ plane to select the most massive galaxies within a passively evolving population, and with a nearly constant number density as a function of redshift up to $z \sim 0.7$ [2, 40]. BOSS spectra are obtained at a resolution R $\sim$ 2000 in the observed wavelength range 3750–10000 Å. Stellar masses for a large BOSS sample have been obtained by ref. [18] through a best fit of the observed photometry. Throughout this work, we considered the estimates obtained assuming a Kroupa initial mass function, accounting for stellar mass losses from stellar evolution. Ref. [41] estimated emission lines properties and stellar velocity dispersions on the same sample.

Starting from BOSS Data Release 9 (DR9), we considered all galaxies with measured stellar masses, emission lines and stellar velocity dispersions, obtaining an original sample consisting of 848697 galaxies for which the D_n4000 index has been measured.

subsample [km/s]	redshift range	σ [km/s]	$\log(M/M_\odot)$	S/N(D_n4000)	# of galaxies
$\sigma \leq 150$	$0.45 - 0.55$	133 ± 17	11.22 ± 0.18	$11.8^{+51.2}_{-5.1}$	5557
$150 < \sigma \leq 200$	$0.32 - 0.65$	182 ± 16	11.25 ± 0.18	$11.9^{+53.9}_{-4.9}$	22710
$200 < \sigma \leq 250$	$0.33 - 0.75$	226 ± 18	11.31 ± 0.19	$12.1^{+53.9}_{-4.9}$	45995
$250 < \sigma \leq 300$	$0.35 - 0.8$	271 ± 17	11.37 ± 0.21	$12.4^{+54.2}_{-5}$	36958
$\sigma > 300$	$0.45 - 0.85$	331 ± 32	11.46 ± 0.22	$12.6^{+57.8}_{-5.2}$	22677

Table 1. Median properties of the sample measured on individual galaxies in each velocity dispersion subsamples.

As discussed in section 2, the "cosmic chronometers" method relies on the selection of an optimal sample of massive and passive galaxies, minimally contaminated by star-forming galaxies outliers. A star-forming population, with its evolving properties (in terms of age, mass, metal content) as a function of cosmic time, could potentially bias the results. On the contrary, as already discussed, the most massive and passive galaxies represent the most homogeneous sample in terms of epoch and timescale of formation, thus being the best tracers of the age of the Universe as a function of redshift. It is therefore of utmost importance to ensure the purity of the sample by removing all galaxies with residual on-going star formation. A combination of selection cuts in color, spectroscopic properties, and stellar mass ($\mathcal{M}_{\rm stars} \gtrsim 10^{10.75}\mathcal{M}_\odot$) has been demonstrated to maximize the purity of such a passively evolving galaxy sample [36].

We therefore applied the following cuts to obtain our sample.

- **Color cut.** We selected galaxies with a color $(g - i) > 2.35$ [18], which was proven to select 'early-type' (passive) galaxies [42].

- **Emission line cut.** We selected galaxies without detectable emission lines, where the main cut has been done on the [OII]λ3727 line, since, given the wavelength range, it is measurable throughout the entire redshift range. We selected galaxies with an equivalent width (EW) EW([OII]) < 5 Å and a signal-to-noise ratio (S/N(EW)) < 2. The sample has been further cleaned by discarding galaxies with significant emission in Hα, [OIII]λ5008 and Hβ, namely at $S/N(EW) > 2$.

- **D_n4000 measurement cut.** To remove low-quality measurements corresponding to spectra with lower S/N, we selected galaxies with an error $\sigma(D_n4000) < 0.25$, obtaining on average a S/N(D_n4000) > 10.

The final sample contains 133912 galaxies, and represents the largest sample of massive and passive galaxies to date, improving current statistics by ∼2 orders of magnitude at these redshifts. This sample was further divided into 5 velocity dispersion bins: $\sigma < 150$, $150 < \sigma < 200$, $200 < \sigma < 250$, $250 < \sigma < 300$, and $\sigma > 300$ km/s. The properties of the various subsamples are reported in Tab. 1, and the stellar mass and redshift distributions are shown in figure 1.

Median stacked spectra have been created for each subsample by co-adding individual spectra in redshift bins of $\Delta z = 0.025$, and the results are shown in figure 2. The redshift binning has been optimized by choosing the smallest width for which the median D_n4000–z

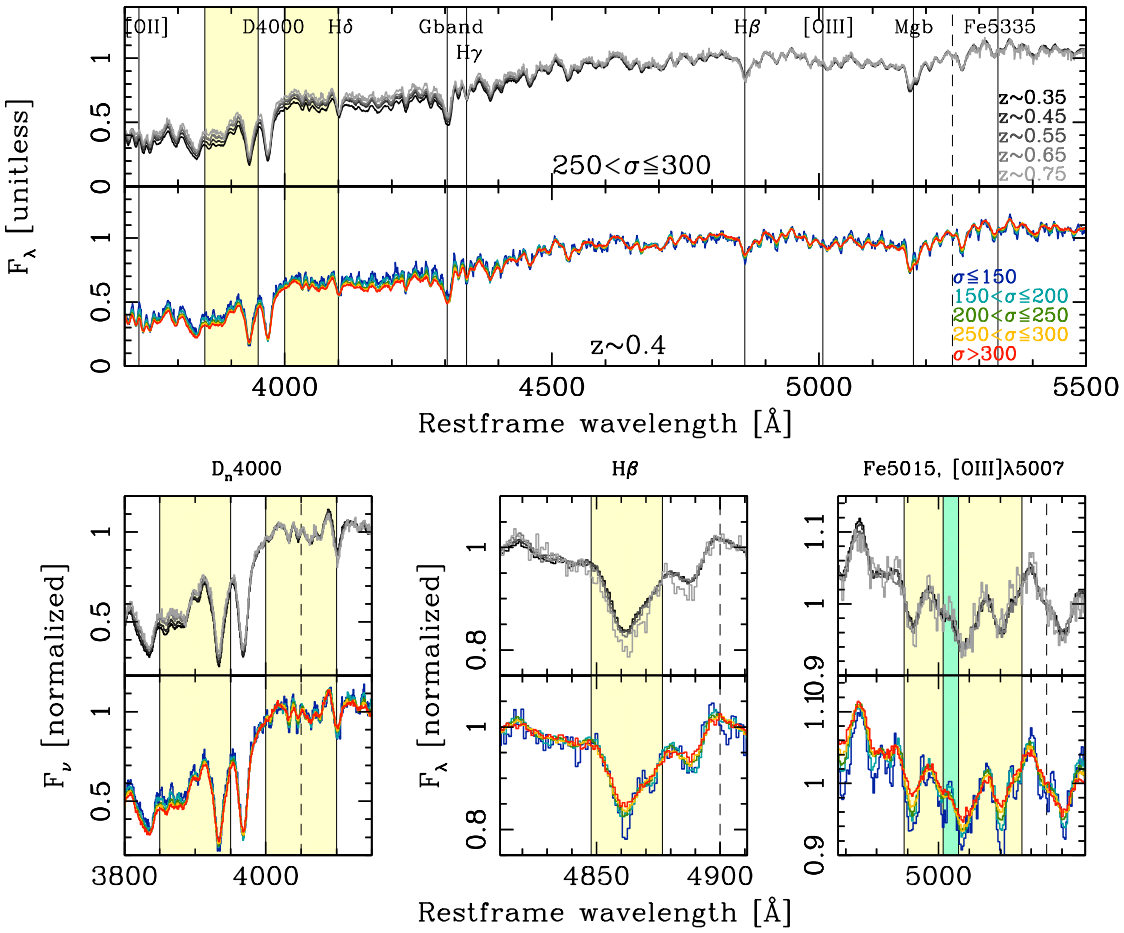

Figure 2. Median stacked spectra as a function of redshift bins and σ bins (the upper and lower panels of each plot respectively). The spectra in the upper panels of each plot are extracted at fixed σ (grey lines, $250 < \sigma < 300$), while the spectra in the lower panels are extracted at fixed redshift (colored lines, $z \sim 0.4$). The upper plots show the median spectra. All spectra have been normalized near to the vertical dashed lines; therefore the differences in the upper panels flatten at higher wavelengths, but the steepening of the slope of the continuum with increasing mass and decreasing redshift is evident. This trend may be interpreted in the framework of the "mass-downsizing" scenario, with more massive galaxies being redder and older than less massive ones. The lower plots are zoom-in around three specific absorption features, i.e. D_n4000, Hβ, and Fe5015, highlighted in yellow; it is also shown, highlighted in green, the region corresponding to [OIII]λ5007 line.

were not noise dominated; the choice of a small binning allows to follow the redshift evolution without excessive smoothing.

The stacked spectra presented in figure 2 are typical of a passive population, with a clear red continuum, characteristic absorption features and no noticeable emission lines, demonstrating the effectiveness of the implemented selection criteria. A zoom-in around three specific lines is shown for D_n4000, Hβ, and Fe5015 respectively. The Hβ absorption line is a feature which is almost independent of metallicity, depending mostly only on the age of the galaxy population, being shallower for high ages. From the visual inspection of

this line the aging of galaxies with cosmic time is evident, with galaxies at higher redshifts being younger. Fe5015 is instead a good proxy of the metallicity of the galaxy; in this case no significant trend with redshift can be noticed, giving a hint of no metallicity evolution of this population with cosmic time. The absence of clearly visible [OIII]λ5007 line shows the purity of the sample, where all contamination from emission-line galaxies has been removed.

4 Analysis

In this section we discuss the methods used to constrain the stellar metallicity Z and to measure and calibrate the D_n4000–z relations.

4.1 Constraining the stellar metallicity

The stellar metallicity Z of the various subsamples has been estimated from full spectral fitting of the median stacked spectra, in bins of redshift and velocity dispersion. The measurements have been performed on the median stacked spectra to increase the S/N from a typical value of about 5/Å for individual galaxies [41] to about $300 - 600$/Å around $\lambda_{\rm rest} = 5000$ Å. Depending on the considered bin, the final spectra were obtained by stacking from ~ 1500 up to ~ 5000 galaxies (Tab. 1). Moreover, in ref. [43] it was verified that the measurement of the metallicity on individual spectra is consistent with the one obtained on median stacked spectra. It is worth also noting that ref. [44] found a general agreement between estimates obtained from full spectral fitting and from other techniques (e.g. Lick indices), and these results have been more recently confirmed by ref. [28].

Different codes have been used to estimate the mass-weighted metallicity, and the results compared to quantify the robustness of the measurements, namely STARLIGHT [45], VESPA [46] and FIREFLY [47]. To further assess the dependence of the results on the assumed parameters, each code has been run adopting two different EPS model, Bruzual & Charlot (2003) (hereafter BC03, [48]) and Maraston & Strömbäck (2011) (hereafter M11, [44]). These two models present substantial differences, such as the treatment of the thermally pulsating asymptotic giant branch phase, the method used to estimate integrated spectra, and the stellar evolutionary models adopted to build the isochrones (for more extensive discussion, see e.g. [44, 49]). Moreover, they are also based on independent libraries of stellar spectra, the latest MILES models [50] for M11 and STELIB [51] for BC03. The M11 models are based on a selection of libraries of empirical stellar spectra (Pickles, ELODIE, and STELIB), but we studied the ones with MILES models to be consistent with the work done in previous analysis [11]. The two models provide similar metallicity ranges for exploration: $Z/Z_\odot = [0.4, 1, 2.5]$ for BC03 and $Z/Z_\odot = [0.5, 1, 2]$ for M11, and have a similar resolution, 3 Å across the wavelength range from 3200 Å to 9500 Å for BC03 [48], and 2.54 Å across the wavelength range from 3525 Å to 7500 Å for M11 [52], similar to BOSS spectra [53].
The full spectral fitting codes applied to estimate the metallicity are described here:

- The full-spectrum fitting code STARLIGHT [45, 54] provides a fit to both the galaxy spectral continuum and spectral features. It simultaneously fits a stellar population mix, which is given as a combination of spectra defined in user-made libraries, the global stellar velocity dispersion and the amount of dust extinction (in terms of A_V). The contribution of each library spectrum to the best fit model is enclosed in the so-called light-fraction and mass-fraction population vectors, which contain, respectively, the light and the mass fractions with which each library model contributes to the best

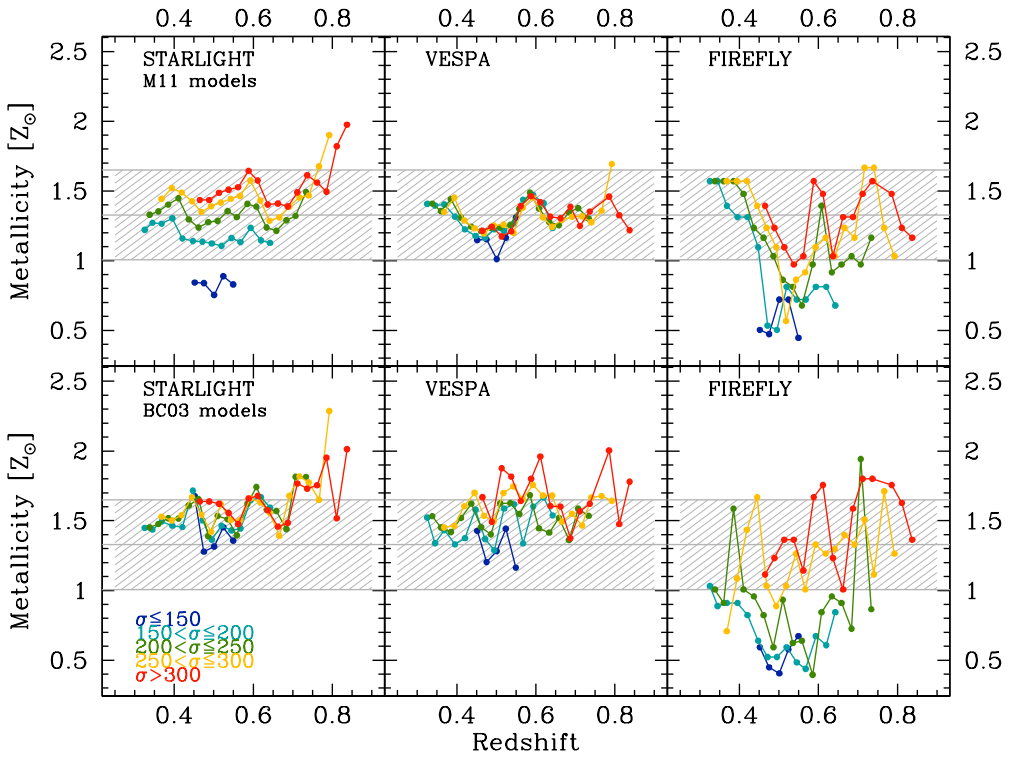

Figure 3. Stellar metallicity estimated from full spectral fitting with STARLIGHT, VESPA and FIREFLY (respectively left, center and right panels), and adopting M11 and BC03 models (respectively upper and lower panels). The grey shaded region represents the mean value, averaged between all models and codes, as discussed in the text.

fit spectrum at a reference wavelength λ. The best fit model is then derived by exploring the parameters space through a mixture of simulated annealing and Metropolis-Hasting Markov Chain Monte Carlo techniques.

- VErsatile Spectral Analysis (VESPA, [46, 55]) is a full spectral fitting code to recover non-parametric star-formation and metallicity histories from optical spectra. VESPA works on a grid of ages logarithmically binned between 0.02 and 14 Gyr with a resolution adaptable to the quality of the data, increasing the resolution only where the data demand it. VESPA imposes no constraints on the amount of star formation or metallicity in each age bin. VESPA finds the best-fit solution by appropriately linearizing the problem and then performing a single matrix inversion to solve the problem. Errors and full covariance matrices are computed by perturbing and then fitting the original best-fit solution a number of times. Dust attenuation is modeled according to either a one or two-parameter mixed-slab dust model of ref. [56].

- FIREFLY [47] is a full spectral fitting code designed to recover galaxy properties and their errors as a function of input model ingredients, such as stellar library, whilst also mapping out stellar population property degeneracies from both the inherent degeneracies in galaxy spectra and errors in the data. It constructs linear combinations of single burst in order to build up complex star formation histories. It has been tested to work

well down to signal-to-noise of 5 [47], and includes an innovative method for treating the effects of dust attenuation and flux calibration through use of Fourier filters. The spectral fitting is adapted to the specific velocity dispersion of the data.

The mass-weighted stellar metallicity estimated for the various ETG subsamples is shown in figure 3. The various fits show on average a slightly over-solar metallicity, with a value $Z/Z_{\odot} \sim 1 - 1.5$. This result is both expected on a theoretical basis, and confirmed by other independent analysis. On a theoretical basis, for galaxies which have fully exhausted their gas reservoir, having completed their mass assembly at high redshift and being passively evolving since then, a negligible evolution in stellar metallicity is expected. Moreover refs. [26, 57, 58, 59, 60] analyzing the Sloan Digital Sky Survey at redshifts $0 < z < 0.3$ similarly found a slightly over-solar metallicity for galaxies with masses $\log(\mathrm{M}/\mathrm{M}_{\odot}) \sim 11$, and these measurements are confirmed also for galaxies of the same mass at much higher redshifts ($z \sim$1.5–2 [61, 62]).

While no statistically significant difference is detectable between the best-fits obtained with the different codes, FIREFLY presents a slightly larger dispersion, that could be due to the fact that it does not assume, as STARLIGHT, a fixed velocity dispersion. A slight difference is present between BC03 and M11 estimates, with BC03 values preferring a metallicity $Z/Z_{\odot} \sim 1.5$ while M11 $Z/Z_{\odot} \sim 1.25$; this difference is due to the intrinsic different input physics and methods in the models, as discussed e.g. in refs. [44, 49]. It is important to notice that all best-fits find a negligible metallicity evolution, in agreement with what found from the visual inspection of the median spectra (see figure 2), confirming that galaxies have been evolving little over the redshift range probed.

To be as conservative as possible, we therefore decided to average the six metallicity estimates obtained with all models and codes, so that the dispersion of the obtained distribution takes all the systematic uncertainties into account. In this way, we obtain a mean value for the stellar metallicity of $Z/Z_{\odot} = 1.35 \pm 0.3$. We verified that this estimate is also stable when calculating the median, or restricting the redshift range, being always compatible within the errorbars.

4.2 Measuring and calibrating the median D_n4000–z relations

For each velocity dispersion subsample, we calculated the median D_n4000 from the individual measurements with a $\Delta z = 0.025$ redshift binning. The associated error has been estimated using the median absolute deviation (MAD), defined as $\mathrm{MAD} = 1.482 \cdot \mathrm{median}(|D_n4000 - \mathrm{median}(D_n4000)|)$, divided by $\sqrt{N}$, i.e. $\sigma_{med}(D_n4000) = \mathrm{MAD}/\sqrt{N}$ [63]. We verified that the median value obtained from the individual galaxies is consistent with the value estimated on the median stacked spectrum in each bin.

Sigma-clipping has been applied to both red and blue D_n4000 bands of the spectrum, to remove contamination of residual night sky emission lines (see figure 9). This method provided results compatible with other approaches, but is more generic and less dependent on various assumptions (see appendix A). The BOSS spectrograph is composed of two separate instruments, a red and a a blue arm, connected at $\lambda \sim 6000$ Å. Any mis-calibration would impact the D_n4000 feature at $z \sim 0.5 - 0.6$. Indeed a strong contamination (not clearly evident by visual inspection, but well detectable in the median relations) persists in all subsamples in the form of a wiggle of the D_n4000–z relations at $0.5 < z < 0.65$. For this reason we decided to restrict our analysis to $z < 0.5$ (see figure 10 in the Appendix). A more detailed discussion can be found in appendix B.

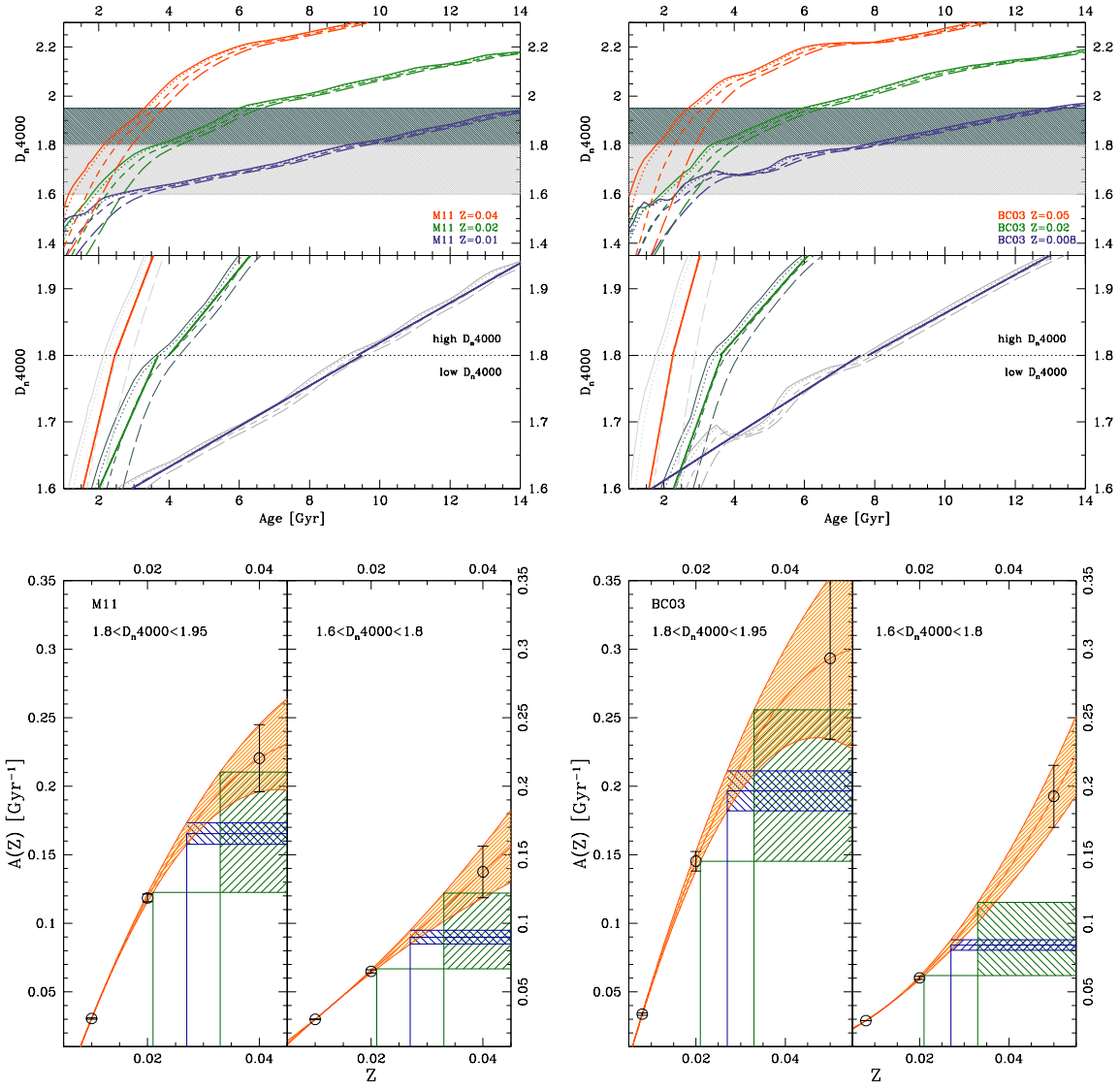

Figure 4. Calibration of the D_n4000-age relations. Upper plots: D_n4000-age relation for different EPS models, metallicities and SFH. Left and right panels show M11 and BC03 models, respectively, where the green lines show the relations for solar metallicity, blue for sub-solar and orange for over-solar; lines from solid to dashed represent SFH with progressively higher τ, from 0.05 to 0.3 Gyr. Lower panel show the linear best fit to each metallicity, in the two D_n4000 ranges discussed in the text. Lower plots: fitted $A(SFH, Z/Z_\odot)$-metallicity relation for different EPS models. The orange shaded area represent the best fit to the data, shown as black points. The green shaded area represent the total error on $A(SFH, Z/Z_\odot)$, given the uncertainty on the measured metallicity, while the blue area show the contribution to the error due to SFH.

The median D_n4000–z relations are shown in the upper panel of figure 5. These relations show a clear pattern, where more massive galaxies present a larger break, confirming what was found in the analysis of ref. [32]. This result can be interpreted in terms of redshift of formation, in particular for the three bins with the higher velocity dispersions where a

		$1.6 < D_n4000 < 1.8$	$1.8 < D_n4000 < 1.95$
M11	$A(Z/Z_\odot = 0.5)$	0.0299 ± 0.0002	0.0305 ± 0.0005
M11	$A(Z/Z_\odot = 1)$	0.065 ± 0.001	0.119 ± 0.003
M11	$A(Z/Z_\odot = 2)$	0.138 ± 0.02	0.22 ± 0.02
BC03	$A(Z/Z_\odot = 0.4)$	0.02893 ± 0.00004	0.037 ± 0.001
BC03	$A(Z/Z_\odot = 1)$	0.0602 ± 0.001	0.145 ± 0.007
BC03	$A(Z/Z_\odot = 2.5)$	0.193 ± 0.002	0.29 ± 0.06

Table 2. $A(SFH, Z/Z_\odot))$ obtained from eq. 2.1 calibrating the D_n4000-age relation (in units of [Gyr^{-1}] for the M11 and BC03 models with different metallicities and for different D_n4000 ranges. The quoted errors are the dispersion between the values evaluated for different SFH choices, as discussed in the text.

smaller difference in metallicity is noticeable. For these samples it can be inferred that more massive galaxies are older and have formed their stellar mass at higher redshifts with respect to less massive ones, providing another observational confirmation to the mass-downsizing scenario [25, 26, 64, 65, 66].

We estimated the quantity $A(SFH, Z/Z_\odot)$ of eq. 2.2 following the approach discussed in ref. [11]. In that work, it was demonstrated that dividing the D_n4000 range into two regimes ($1.6 < D_n4000 < 1.8$ and $1.8 < D_n4000 < 1.95$), the approximation of a linear relation between D_n4000 and age is extremely accurate independently of the considered model. In particular, for each EPS model three metallicities (sub-solar, solar and over-solar) and four different SFHs (characteristic of the selected passive population, i.e. a delayed exponentially declining SFH has been chosen, with $\tau = 0.05, 0.1, 0.2, 0.3$ Gyr) are considered, and, at fixed metallicity, the slope of the D_n4000–age relation is obtained by averaging the values obtained for the various SFHs. The dispersion between the different SFHs has been taken into account as the associated error to $A(SFH, Z/Z_\odot)$; then, the obtained values are interpolated to obtain the correct $A(SFH, Z/Z_\odot)$ parameter at the metallicity of the sample.

The results for M11 and BC03 models are listed in Tab. 2 and shown in Fig. 4. The upper panels show the D_n4000–age relations at different metallicities and SFHs for both M11 and BC03 models. As it is evident from the bottom panels of the upper plots, in both D_n4000 ranges the linear fit to the data represent a very good approximation, with Spearman correlation coefficients always above 0.97, and on average of $\langle r \rangle = 0.995 \pm 0.002$ in the lower D_n4000 range and $\langle r \rangle = 0.9985 \pm 0.0003$ in the higher D_n4000 range for M11, and of $\langle r \rangle = 0.989 \pm 0.003$ and $\langle r \rangle = 0.9987 \pm 0.0004$ for BC03, respectively in the lower and higher D_n4000 range. The lower panels of Fig. 4 show the factor $A(SFH, Z/Z_\odot)$ as a function of the metallicity, and the interpolation performed. Green and blue shaded area represent the total uncertainty on $A(SFH, Z/Z_\odot)$ (given the metallicity range as measured from our sample, see Sect. 4.1), and the contribution due to SFH alone. It is clear that the dominant systematic is at the moment due to our uncertainty on stellar metallicity, which contributes to ∼80% of the systematic error budget in M11, and to ∼75-85% in BC03, depending on the D_n4000 range.

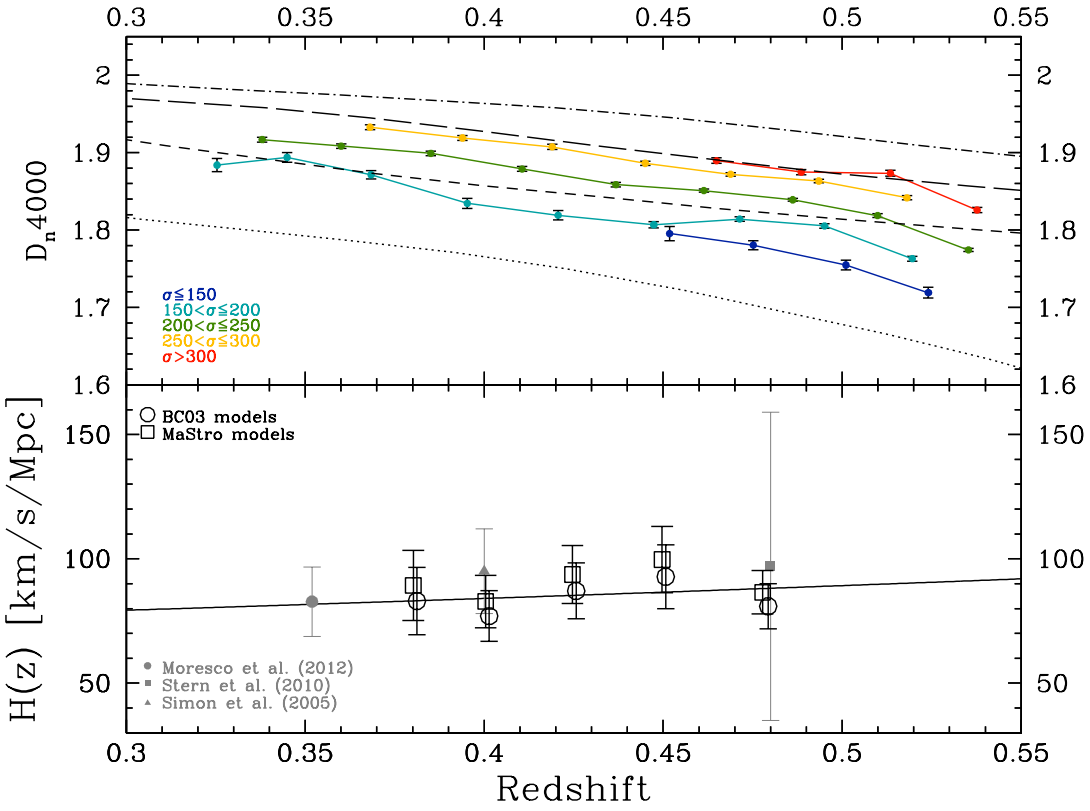

Figure 5. Upper panel: median D_n4000–z relations obtained for the various velocity dispersion subsamples. The dashed lines show the theoretical D_n4000–z relations estimated from M11 models (with solar metallicity) for four differed redshifts of formation, respectively 1, 1.5, 2, 2.5 from bottom to top. Lower panel: $H(z)$ measurements obtained with BC03 and M11 models, compared with literature data available in this redshift range [11, 12, 13]. For illustrative purpose, the estimates obtained with BC03 models have been slightly offset in redshift.

5 Results

5.1 The estimate of $H(z)$

We estimated the Hubble parameter $H(z)$ from eq. 2.2. To keep under control the systematic uncertainties, we performed the analysis separately with two different EPS models, BC03 and M11, and then compared the results. The method to estimate $A(SFH, Z/Z_\odot)$ has been discussed in section 4.2. The stellar metallicity has been taken from the analysis presented in section 4.1, $Z/Z_\odot = 1.35 \pm 0.3$. The differential dz/dD_n4000 has been obtained from the median D_n4000–z relation presented in the upper panel of figure 5, considering the difference between the i-th and the $(i+N)$-th point for each velocity dispersion subsample. We have chosen $N = 4$ as a trade-off to minimize the statistical scatter of the data over the intrinsic D_n4000 evolution with redshift, simultaneously maximizing the redshift sampling of $H(z)$. We therefore consider a redshift interval $\Delta z = 0.1$, which corresponds to a difference in cosmic time ~ 0.7 Gyr at $z \sim 0.45$. We checked that different choices of N (provided not to be dominated by the statistical scatter of the data) do not affect the results.

The $H(z)$ measurements extracted from the different σ subsamples are in good agree-

	M11 models					BC03 models				
z	$H(z)$	σ_{stat}	σ_{syst}	σ_{tot}	% error	$H(z)$	σ_{stat}	σ_{syst}	σ_{tot}	% error
0.3802	89.3	3.2	13.7	14.1	15.8%	83.0	4.3	12.9	13.5	16.3%
0.4004	82.8	2.4	10.3	10.6	12.8%	77.0	2.1	10	10.2	13.2%
0.4247	93.7	2.7	11.4	11.7	12.4%	87.1	2.4	11	11.2	12.9%
0.4497	99.7	3.1	13	13.4	13.4%	92.8	4.5	12.1	12.9	13.9%
0.4783	86.6	2	8.5	8.7	10.1%	80.9	2.1	8.8	9	11.2%
$\langle 0.4293 \rangle$	91.8	1	5.1	5.3	5.8%	85.7	1	5.1	5.2	6.1%

Table 3. $H(z)$ measurements (in units of [km/Mpc/s]) and their errors. The relative contribution of statistical and systematic errors are reported, as well as the total error (estimated by summing in quadrature σ_{stat} and σ_{syst}). These values have been estimated with M11 and BC03 EPS models respectively. For each model the averaged measurement is also reported. This dataset can be downloaded from http://www.physics-astronomy.unibo.it/en/research/areas/astrophysics/cosmology-with-cosmic-chronometers.

ment, and, being statistically independent, they have been combined together averaging them in bins of $\Delta z = 0.025$; we use a weighted mean where the weights are the corresponding error of each measurement. The results are shown in figure 5, and presented in Tab. 3. Exploiting BOSS data, we are able to map homogeneously for the first time the redshift range $0.3 < z < 0.5$ with an accuracy between 11% and 16%, which, as can be seen by figure 5, was previously only poorly covered. The comparison between the results obtained with the two different EPS models also shows a good agreement, always $< 1\sigma$, confirming the robustness of the estimate as found in ref. [11]. Despite the larger statistic of this analysis with respect to the one of ref. [11], however, we have similar errorbars. This is due to the fact that in this work we have larger uncertainty on the slope dz/dD_n4000 since we are using smaller redshift arm ($\Delta z = 0.1$ instead of 0.3). Precise measurements in this redshift range are crucial to better constrain the time at which our Universe passed from decelerated to accelerated expansion.

Analyzing Tab. 3, it is clear that, with the exceptional statistics provided by the BOSS data, systematics are now dominating over statistical errors. Since the systematics themselves are mainly dominated by the uncertainty on metallicity and by the EPS model, additional work is needed to improve on the current analysis. We plan to address this issue by exploiting the present dataset in a following paper, with a full and detailed spectral analysis.

To exploit the full constraining power of BOSS data, we decide also to provide a single $H(z)$ measurement, in which all mass subsamples have been averaged as discussed above, but in a single point. This measurement is clearly not independent of the results reported in Tab. 3, and should not be used in combination with them. The resulting constraint adopting M11 models is $H(z = 0.4293) = 91.8 \pm 5.3$ km/s/Mpc, and $H(z = 0.4293) = 85.7 \pm 5.2$ km/s/Mpc using BC03 models, reaching a 6% accuracy including both statistic and systematic errors. As a comparison, we report the results obtained from the BAO analysis in the final BOSS DR12 [71], where it is found $H(z = 0.57) r_{\rm d}/r_{\rm d}^{\rm fid} = 100.3 \pm 3.7$ km/s/Mpc and $H(z = 0.32) r_{\rm d}/r_{\rm d}^{\rm fid} = 79.2 \pm 5.6$ km/s/Mpc. Considering that $r_{\rm d}^{\rm fid} = 147.10$ Mpc and $r_{\rm d} = 147.41 \pm 0.30$ from Planck analysis [9], these measurements correspond to $H(z = 0.57) = 100.1 \pm 3.7$ and $H(z = 0.32) = 79.0 \pm 5.6$km/s/Mpc, respectively a 3.7% and 7.1% measurement.

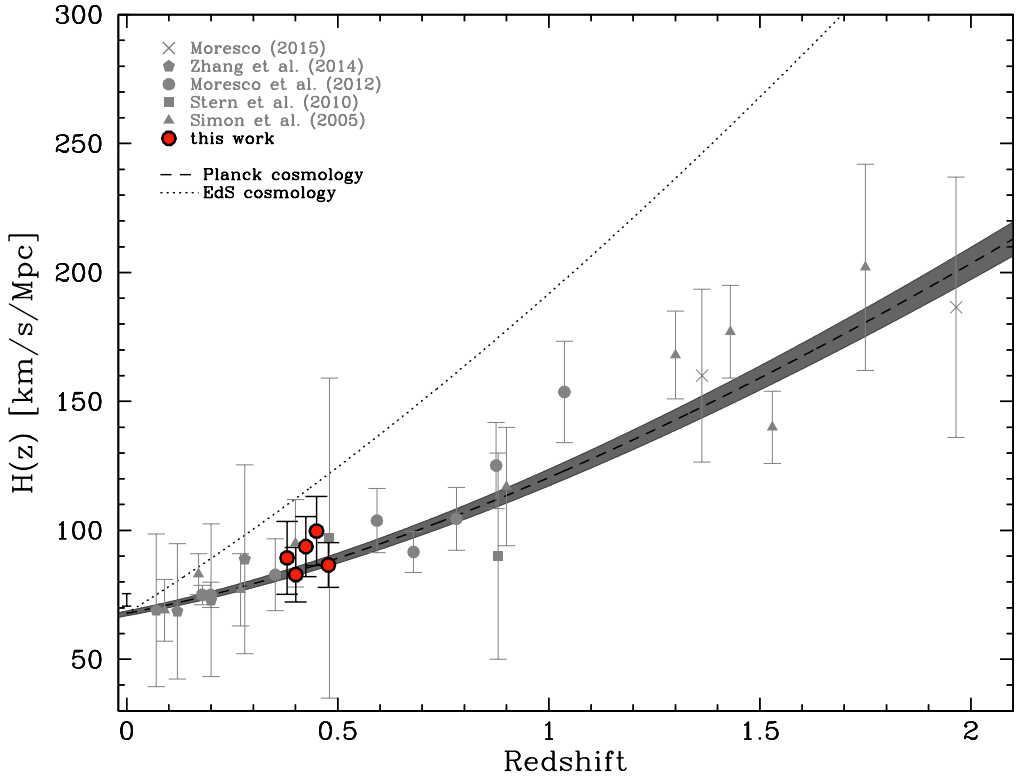

Figure 6. Hubble parameter constraints obtained with M11 models, compared with various literature data [11, 12, 13, 67, 68]. The black point at $z = 0$ is the Hubble constant constraints from ref. [69] with the recalibration of the distance to NGC 4258 from ref. [70], i.e $H_0 = 73 \pm 2.4$ km/s/Mpc. The solid line and the dashed regions are not a fit to the data, but show the fiducial flat ΛCDM cosmology with its 1σ uncertainty as constrained by Planck collaboration ([9], $H_0 = 67.8 \pm 0.9$ km/s/Mpc, $\Omega_m = 0.308 \pm 0.012$). For comparison an Einstein-de Sitter model is shown, normalized to the same H_0.

5.2 The measurement of the transition redshift

The cosmological transition redshift z_t is defined as the redshift which separates the accelerated and decelerated expansion phases of the Universe. The BOSS data map the redshift range close to this epoch of cosmic re-acceleration homogeneously for the first time, and therefore allow us to measure it with cosmic chronometers with high accuracy. We constrained z_t by fitting all the "cosmic chronometers" data available so far in the literature [11, 12, 13, 67, 68], including the ones obtained in this work, with a standard χ^2 approach. In this analysis, we have considered the measurements obtained assuming BC03 models, for consistency with literature derivations, as presented in Tab. 4 and figure 6.

The transition redshift determination can be done in the standard (model-dependent) way, assuming a Friedmann-Robertson-Walker metric and general relativity (i.e. ΛCDM-like cosmological model), and in a model-independent way.

First of all, we consider an open ΛCDM cosmology:

$$H(z) = H_0 \left[\Omega_m (1+z)^3 + \Omega_k (1+z)^2 + \Omega_\Lambda\right]^{1/2}, \tag{5.1}$$

where $\Omega_k = 1 - \Omega_m - \Omega_\Lambda$. The transition redshift can be written as:

$$z_t = \left[\frac{2\Omega_\Lambda}{\Omega_m}\right]^{1/3} - 1. \tag{5.2}$$

Combining equations 5.1 and 5.2, we obtain a relation $H(z)_{mod} = f(H_0, \Omega_m, z_t)$. We assumed a gaussian prior on the Hubble constant $H_0 = 73 \pm 2.4$ km/s/Mpc [69, 70, 71], which is a cosmology-independent, direct measurement. For the other parameters, we considered uniform priors $\Omega_m \in [0, 1]$ and $z_t \in [0, 1.5]$. The results are presented in figure 7: in the left panel the one-dimensional marginalized χ^2 for z_t is shown, while the right panel shows the two-dimensional constraints in the $\Omega_m - z_t$ plane.

We obtained $z_t = 0.64^{+0.11}_{-0.07}$, which is in good agreement with Planck (2015) results [9] assuming an open ΛCDM cosmology[1], as shown in figure 7. Our measurement is slightly larger than the estimate from ref. [19] ($z_t = 0.43^{+0.27}_{-0.08}$ at 95% confidence level) obtained using SNe, and more consistent with the larger value of ref. [20] ($z_t = 0.73^{+0.45}_{-0.13}$ at 95% confidence level), and with the estimate provided by the analysis of BAO in the Lyα forest of BOSS quasars ($z_t \sim 0.7$, [72]). This result is in good agreement with the estimate from an independent fit to SNe of ref. [22], providing $z_t = 0.643^{+0.034}_{-0.030}$ with a class of models deviating from GR (assuming $\Omega_m = 0.315$). Ref. [21] analyzed the constraints on another class of $f(R)$ gravity models, and by combining SNe, BAO and older $H(z)$ measurements they obtained $z_t = 0.7679^{+0.1831}_{-0.1829}$. Refs. [73, 74], analyzing older $H(z)$ measurements in combination with BAO measurements in different cosmological scenarios, found a mean value of $z_t = 0.74 \pm 0.05$. Recently, also ref. [75] analysed the age of galaxies, strong lensing and SNe obtaining a constraint on $z_t < 1$, considering both a parametric and a non-parametric approach. Note that previous results were obtained from the analysis of SNe, comprising SNLS and Union2 samples, BAO and from the latest CMB measurements from Planck satellite, while in our case the measurement comes only from cosmic chronometers data and the local $H(z)$ measurement.

The transition redshift can be also constrained without any further assumption from the function $f(z) = H(z)/(1+z) = \dot{a}$, that directly maps the acceleration of the Universe. This function has a positive slope when the Universe is accelerating, and a negative slope when it is decelerating. The deceleration parameter q is related to $f(z)$ by $q = -H(z)/f(z)$. Our measurements are crucial to provide the first cosmology-independent determination of the redshift of transition between decelerated and accelerated expansion, z_t, at high statistical significance. Combining them with literature data as presented in Tab. 4 and adopting the most recent local distance ladder measurement of the Hubble constant H_0 [69, 70, 71], which is also independent of any cosmology-based constraint, we obtain 31 $H(z)/(1+z)$ measurements (see figure 8). We fit these data with a piecewise linear function composed of two intervals (one for acceleration and one for deceleration), which is the simplest functional form parameterizing a change in the slope of $H(z)/(1+z)$ without assuming any model. The transition redshift between the two regimes is a free parameter, together with the slope of the two lines and the overall amplitude. We use a standard χ^2 approach, and, marginalizing over all other parameters, we find a transition redshift of $z_t = 0.4 \pm 0.1$ at the 68% confidence level, as shown in figure 8. We have also explored fitting with other functional forms like a parabola and a spline; however, the piecewise function provides the best χ^2 and the transition redshift does not change within the 68% confidence limit.

We also attempt a fit to the data with a straight-line, where no transition between decelerated and accelerated expansion is assumed, and compare the results. The BOSS data

[1] see http://wiki.cosmos.esa.int/planckpla2015/index.php/Cosmological_Parameters.

continues

z	$H(z)$	$\sigma_{H(z)}$	ref.	z	$H(z)$	$\sigma_{H(z)}$	ref.
0.07	69.0	19.6	[67]	0.4783	80.9	9	this work
0.09	69	12	[12]	0.48	97	62	[13]
0.12	68.6	26.2	[67]	0.593	104	13	[11]
0.17	83	8	[12]	0.68	92	8	[11]
0.179	75	4	[11]	0.781	105	12	[11]
0.199	75	5	[11]	0.875	125	17	[11]
0.20	72.9	29.6	[67]	0.88	90	40	[13]
0.27	77	14	[12]	0.9	117	23	[12]
0.28	88.8	36.6	[67]	1.037	154	20	[11]
0.352	83	14	[11]	1.3	168	17	[12]
0.3802	83	13.5	this work	1.363	160	33.6	[68]
0.4	95	17	[12]	1.43	177	18	[12]
0.4004	77	10.2	this work	1.53	140	14	[12]
0.4247	87.1	11.2	this work	1.75	202	40	[12]
0.44497	92.8	12.9	this work	1.965	186.5	50.4	[68]

Table 4. $H(z)$ measurements (in units [km/s/Mpc]) used for the cosmological analysis, and their errors.

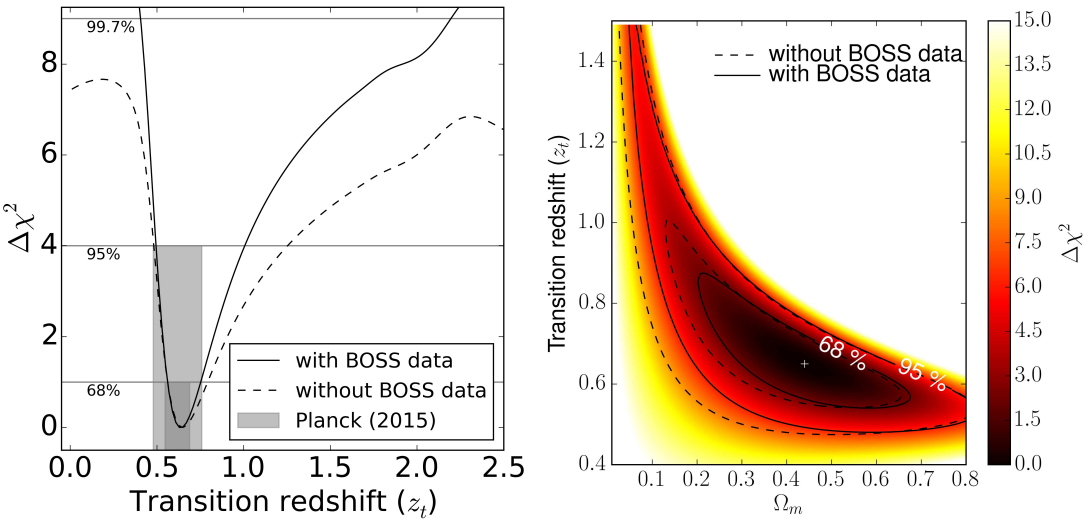

Figure 7. Constraints on the cosmological transition redshift obtained in a oΛCDM cosmology. The left panel shows the effective $\Delta\chi^2$ as a function of z_t. The solid line shows the constraint obtained with the data of Tab. 4, while the dashed line shows the constraint obtained without the values obtained in this work. As a comparison, the grey shaded area represent the 1σ and 2σ constraints from Planck (2015) for an oΛCDM cosmology. In the right panel the 68% and 95% two-dimensional constraints are shown in the $\Omega_m - z_t$ plane, both with and without the new $H(z)$ data obtained in this analysis.

have proven to be crucial for the detection of the transition redshift in both model-dependent and model-independent measurements, as it is evident from figure 7 and 8. For the piecewise

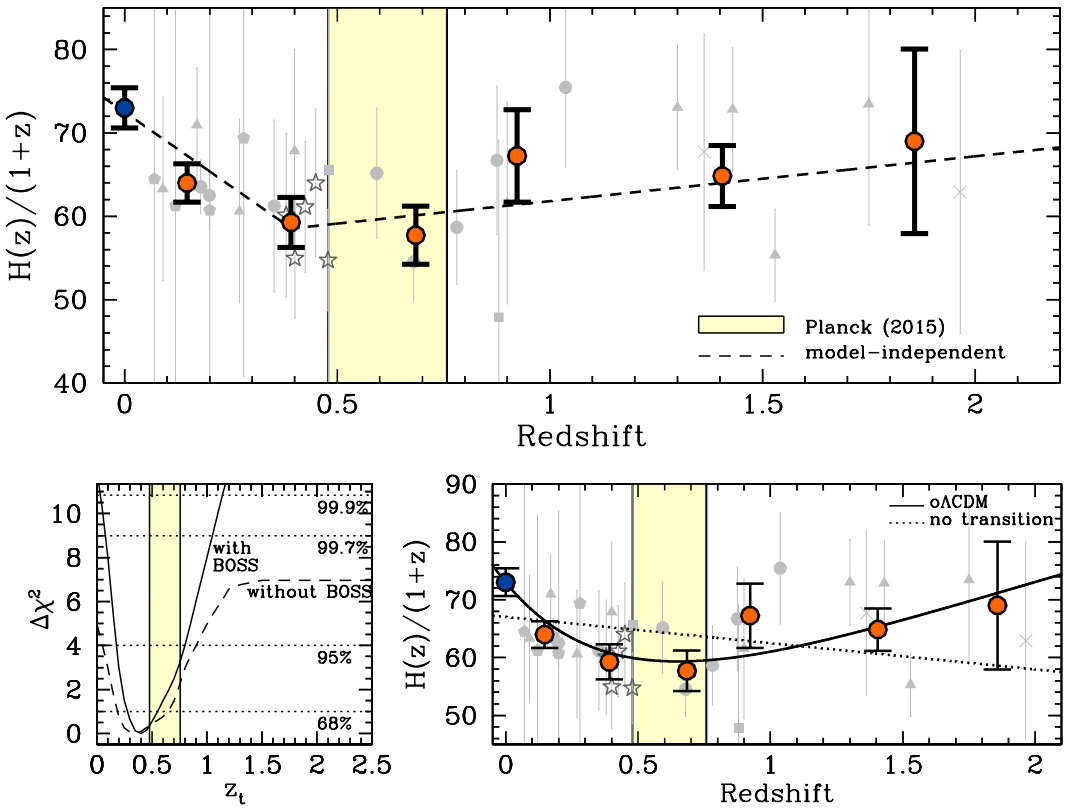

Figure 8. Constraints on the cosmological transition redshift obtained in a model-independent way. In the upper panel are shown the fitted $H(z)/(1+z)$ measurements in grey, with the same coding of figure 6, where the starred symbols are the measurements obtained from this analysis; for this fit we used BC03 measurements for homogeneity with the estimates obtained in literature data. Orange points show the binned values, for illustrative purposes; the analysis is performed on unbinned data. The H_0 value used in this analysis is plotted in blue. The transition from decelerated to accelerated expansion is clearly visible by eye as a turn in the slope of the data. The solid line represents the best fit to the data with a cosmology-independent piecewise linear function. As a comparison, model dependent 2σ constraints obtained from Planck (2015) [9] in an open ΛCDM cosmology are shown in yellow. In the lower-left panel the effective $\Delta\chi^2$ is shown as a function of z_t, with and without considering the new BOSS data; the improvement of the statistical significance of the result provided by the new data is clearly evident. In the lower-right panel are presented for comparison the best fits obtained for the oΛCDM model and for the model without a transition redshift.

fit, without the new BOSS data we obtain no constraint on the transition redshift at a significance of 2.6σ or higher within the redshift range probed by our sample, while on the contrary, considering the new data we find that the transition redshift for the piecewise fit is $0.2 < z_t < 0.8$ at 2σ (95%) and $0.1 < z_t < 1.05$ at 3σ (99.7%) levels, with a detection of $0 < z_t < 1.15$ at 99.9% confidence level. Similarly, for the oΛCDM fit we obtain no constraint at the 3σ level (99.7%) without the new data (with $z_t < 3.5$), and $0.41 < z_t < 2.2$ considering them, proving that BOSS data are necessary for a significant detection.

Different estimators have been proposed in the literature to select the best model fitting

model	assumption	result	AICc	BIC
oΛCDM	cosmology	$z_t = 0.64^{+0.1}_{-0.06}$	21.41	25.71
piecewise linear fit	model-independent	$z_t = 0.4 \pm 0.1$	23.99	28.72
linear fit	model-independent	–	32.42	35.29

Table 5. Constraints on the cosmological transition redshift z_t obtained by fitting cosmic chronometer data with different models. The results are presented at 68% confidence level; all constraints assume a gaussian prior on the Hubble constant $H_0 = 73 \pm 2.4$ km/s/Mpc [69, 70, 71].

a set of data; among them, the most common are the Akaike Information Criterion (AIC, [76]), and the Bayesian Information Criterion (BIC, [77]). These criteria indicate which is the model preferred by data, and the level of confidence at which other models can be discarded, implementing an "Occam razor" selection that penalizes increasing the number of parameters. In this way, they penalize over-fitting the data (for more details, see [78]). Given k degrees of freedom in a model, and N data points, they are defined as:

$$AIC = -2\ln\mathcal{L}_{max} + 2k, \qquad BIC = -2\ln\mathcal{L}_{max} + k\ln \mathrm{N}. \tag{5.3}$$

The BIC penalizes an increased number of free parameters more than AIC; moreover, ref. [79] proposed a correction to AIC which is more correct for finite number of data points:

$$AIC_c = AIC + \frac{2k(k+1)}{N-k-1}. \tag{5.4}$$

Different models are then compared in terms of their ΔAIC_c or ΔBIC based on the Jeffreys' scale [80], so that a difference > 5 is highly significant. In tab. 5 are summarized the results. With both estimators, we find that the model preferred by the data is the oΛCDM, but without significant difference with respect to the cosmology-independent linear piecewise fit. On the contrary, a straight-line is strongly disfavored by the data, both considering AIC_c and BIC. The model with a transition redshift is preferred at highly significant level compared to a model with no transition redshift, therefore ruling out the null hypothesis of no redshift of transition at 99.9% confidence level.

We have shown that the choice of stellar population models does not affect the derived $H(z)$ value and that differences are always smaller than 1σ. However, this small systematic shift might have a larger impact in computing the transition redshift, as it is, effectively, a derivative of $H(z)$. In our data-set only 15 $H(z)$ measurements are derived with M11 models. For this sub-set, following the same approach described in section 5.1, we find $z_t = 0.75 \pm 0.15$ (we note, however, that at 95% confidence level the constraints degrade considerably because of the reduced number of points, giving $0.1 < z_t < 2$). As a further test, we also explored the full BC03 dataset, but using instead M11 $H(z)$ measurements where available. This could be thought as an extreme example of systematic impact, as one should use just a given EPS model where the homogeneity of the EPS model ensures that these differences cancel out when estimating the derivative. In this case, we find $z_t = 0.75 \pm 0.15$ and $0.25 < z_t < 1.0$ at 95% confidence. This is perfectly consistent with our BC03 determination, but with a larger errorbar at higher redshifts. When using Bayesian evidence to analyze the significance of excluding the hypothesis of no transition redshift with this latest data-set, which combines estimates from different EPS models, we find a substantial-strong evidence in agreement with our general analysis. Our conclusion is that even an inhomogeneous analysis of the data provides a significant evidence for a transition redshift between deceleration and acceleration.

6 Conclusions

In this paper, we analyzed BOSS data to set constraints on the expansion history of the Universe through the "cosmic chronometers" approach. We implemented the technique suggested in refs. [11, 32], in which it was proposed to constrain the Hubble parameter $H(z)$ from the differential evolution of a spectral feature, the D_n4000, of very massive and passive galaxies.

The main conclusion of this analysis can be summarized as follows:

- We implement a strict selection criterion to extract, amongst BOSS-DR9, the most massive and passive sample, the least biased by star-forming emission-lines outliers. In this way we select more than 130000 massive and passive galaxies, which are binned in narrow redshift bins to follow the evolution of this population with cosmic time, and in velocity dispersion bins to follow this evolution in different mass bins.

- For all the galaxies of our sample, we measure the D_n4000. We also create median stacked spectra in all the velocity dispersion and redshift bins, which are analyzed with a full spectral fitting technique to extract information on the stellar metallicity of the samples. We apply three different full spectral fitting codes using two EPS models (BC03 and M11), to explore the dependence of the constraints on both the software implemented and the model adopted. These codes yield comparable results, suggesting for our sample an average metallicity of $Z/Z_{\odot} = 1.35 \pm 0.3$, in agreement with other independent estimates for this population of galaxies.

- The inspection of the median D_n4000–z relation provides evidence supporting the mass-downsizing scenario, with more massive galaxies having a larger break and, given the metallicity constraints obtained, older ages with respect to less massive galaxies.

- These measurements are used to obtain five new cosmology-independent $H(z)$ constraints in the redshift range $0.3 < z < 0.5$, with an accuracy ∼11-16%, taking into account both statistical and systematic error. These constraints are obtained adopting two different EPS models, BC03 and M11, to study the dependence of our results on models, finding no significant difference. These new constraints allow us to homogeneously map for the first time this range of cosmic times, which are crucial to disentangle the epoch which separates the decelerated and accelerated phases of the expansion of the Universe.

- To exploit the constraining power of BOSS data, we combine the five measurements, obtaining a constraint $H(z = 0.4293) = 91.8 \pm 5.3$ km/s/Mpc using M11 models, and $H(z \sim 0.43) = 85.7 \pm 5.2$ km/s/Mpc using BC03 models, a 6% measurement including both statistical and systematic errors. This result is a complementary and cosmology-independent result that is comparable to the result obtained from the analysis of BAO from the final BOSS-DR12 sample [71].

- We use the new data obtained, jointly with other cosmic chronometers literature data, to set constraints on the cosmological transition redshift, considering an open ΛCDM cosmology. We obtain a value $z_t = 0.64^{+0.11}_{-0.06}$ in perfect agreement with the estimate from Planck (2015) [9] and SNe [20, 21, 22] analyses.

- The new data from SDSS-III/BOSS allow us to implement also an independent fit to the function $H(z)/(1+z)$, which directly probes the acceleration of the Universe, using a functional form without any further cosmological assumption. In this way, we obtain the constraint $z_t = 0.4 \pm 0.1$. At 99.9% confidence level, this analysis yield a detection of the transition redshift as $0 < z_t < 1.15$, ruling out a straight-line fit, which would imply no transition from deceleration to acceleration, at very high significance. This is the first time that the epoch of cosmic re-acceleration has been observed in a cosmological model-independent way.

This work has shown the potential of the *cosmic chronometers* approach to set cosmology-independent constraints on the Hubble parameter $H(z)$. This technique can be considered as a complementary tool with respect to more standard ones (e.g. BAO, SNe) to set constraints on cosmological models, and to keep the systematic affecting each probe under control. While it has been demonstrated that in many cases the constraining power of this method is comparable with the power of classical approaches, we also note that at the present status the measurements are systematic-dominated. Looking towards the future, on one hand we foresee that an improvement in the measurement of metallicity of passive galaxies will represent a decisive step to minimize systematics, and significantly reduce errorbars; on the other hand, it will be crucial to improve the samples at $z > 0.5$, in order to maximize the accuracy of the measurements over a larger redshift range. From this point of view, future missions like Euclid [81], WFIRST [82], DESI [83] and LSST [84] will represent an ideal starting point at these high redshifts.

In future papers, we plan to explore the capability of these new data, in combination with Planck (2015) measurements, to set constraints on parameters in different cosmological scenarios, focusing on the additional constraining power provided by cosmic chronometers data, and to take advantage of the high-quality stacked spectra obtained in this analysis to set evolutionary constraints on the properties of passive galaxies.

Acknowledgments

MM, LP and AC acknowledge financial contributions by grants ASI/INAF I/023/12/0 and PRIN MIUR 2010-2011 "The dark Universe and the cosmic evolution of baryons: from current surveys to Euclid".

RJ and LV thank the Royal Society for financial support and the ICIC at Imperial College for hospitality while this work was being completed. LV is supported by the European Research Council under the European Community's Seventh Framework Programme FP7-IDEAS-Phys.LSS 240117. Funding for this work was partially provided by the Spanish MINECO under projects AYA2014-58747-P and MDM-2014-0369 of ICCUB (Unidad de Excelencia "Maria de Maeztu")

Funding for SDSS-III has been provided by the Alfred P. Sloan Foundation, the Participating Institutions, the National Science Foundation, and the U.S. Department of Energy Office of Science. The SDSS-III web site is http://www.sdss3.org/.

SDSS-III is managed by the Astrophysical Research Consortium for the Participating Institutions of the SDSS-III Collaboration including the University of Arizona, the Brazilian Participation Group, Brookhaven National Laboratory, Carnegie Mellon University, University of Florida, the French Participation Group, the German Participation Group, Harvard University, the Instituto de Astrofisica de Canarias, the Michigan State/Notre Dame/JINA Participation Group, Johns Hopkins University, Lawrence Berkeley National Laboratory,

Max Planck Institute for Astrophysics, Max Planck Institute for Extraterrestrial Physics, New Mexico State University, New York University, Ohio State University, Pennsylvania State University, University of Portsmouth, Princeton University, the Spanish Participation Group, University of Tokyo, University of Utah, Vanderbilt University, University of Virginia, University of Washington, and Yale University.

A Correcting for night sky emission lines residuals

Night sky line residuals can be important source of noise in (BOSS) spectra. As discussed here and within the BOSS collaboration[2], the lines at 5577 Å, 6300 Å, and 6363 Å in particular may leave significant spikes in the spectra, and bias the measurement of the break if they happen to be in D_n4000 red or blue band. Together with the previous lines, we identify in sky spectra five additional lines with significant residuals at 5892 Å, 5917 Å, 5934 Å and 5955 Å, as shown in figure 9. These residuals bias the measurement of D_n4000, leaving an imprint in the median D_n4000–z relation in the form of wiggles (particularly at $z \sim 0.4$) that depart from the expected theoretical behavior, as can be seen in the left plot of figure 10. To overcome this issue, we applied a sigma-clipping procedure to the observed spectra in the

[2]See https://www.sdss3.org/dr9/spectro/caveats.php#night_sky.

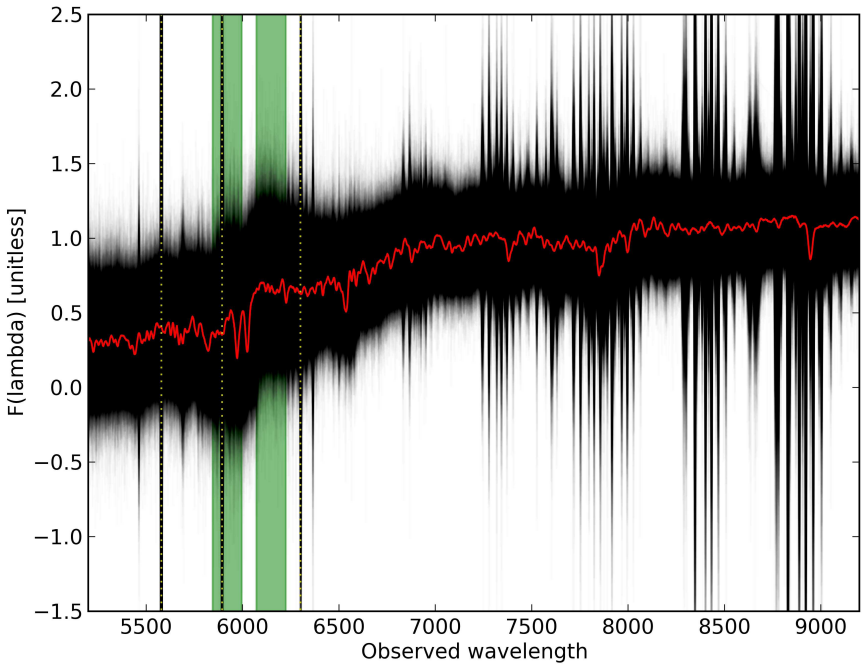

Figure 9. Example of median stacked spectrum (in the observed frame) at $z = 0.5181$ for the subsample with $250 < \sigma < 300$ km/s. The median spectrum is shown in red, while in black are superimposed all the spectra used to create the stack. Particularly evident are the residual of the 5577 Å, of the 5892 Å and of the 6300 Å lines, highlighted with the yellow dotted lines. In green are shown the regions of the red and blue bands of the D_n4000.

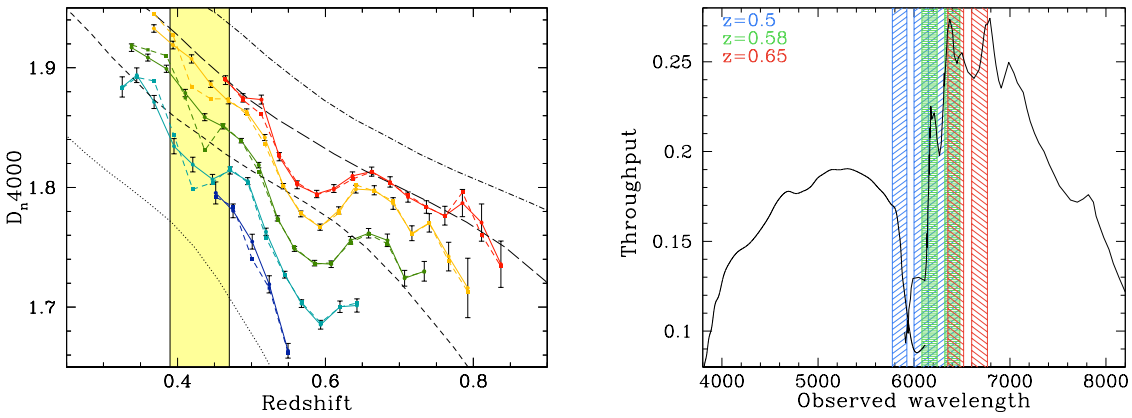

Figure 10. In the left plot is shown the median D_n4000–z relation before (open points, dotted lines) and after (filled points, solid lines) the sigma clipping correction; the correction is in particular effective around $z \sim 0.4$, where the 5577 Å line enters the D_n4000 range. As in figure 5, dashed lines show D_n4000 from models. In the right plot are presented the throughput curves for the red and blue arms of BOSS spectrograph ([53], see also http://www.sdss.org/dr12/algorithms/spectrophotometry/) as a function of observed wavelength. The shaded regions with the same colors highlight the left and right bands where D_n4000 is calculated, at three different redshifts ($z = 0.5$ in red, $z = 0.58$ in green, adn $z = 0.65$ in blue) around which the wiggle in the median D_n4000–z relations is observed, showing that at these redshifts the D_n4000 transits from the blue to the red arm of the spectrograph.

red and blue bands of D_n4000, removing pixels with a $> 4\sigma$ difference from the mean. This helps in particular to remove the wiggle at $z \sim 0.4$, where the strong 5577 Å line falls in the D_n4000 range.

We also explored different methods to clean the spectra from the residuals of the sky emission lines, namely cutting the contaminated pixels, and weighting the pixels with their variance. Each method gave similar results to the one obtained with the sigma clipping approach, being however more dependent on various assumptions (such as how many pixels to cut, how to treat the removed regions, and how to properly weight the pixels). We therefore decide to adopt the first method, and applied it to the data.

B BOSS throughput analysis

The BOSS spectra are obtained with two separate instruments, a blue arm and a red arm, with an overlapping region around ∼6000 Å, as shown in the right plot of figure 10. This observed range falls exactly in the D_n4000 range, once redshifted at $z \sim 0.5$, and in particular we notice a correlation between the descending and ascending trend of the wiggle (described in Appendix A) and the D_n4000 being measured on the blue arm, in the red arm, or in between (see right plot of figure 10). This correlation suggests a possible sub-optimal calibration between the two spectrographs, that results in the observed wiggle in the median D_n4000–z relation. Even if this wiggle is actually small, of the order of $\Delta D_n4000 \sim 0.05$, it significantly affects the $H(z)$ measurement, that critically depends on the differential dD_n4000. In order to avoid biasing our measurements, we therefore decided to restrict our analysis to $z < 0.5$.

References

[1] D. Schlegel, M. White, and D. Eisenstein, "The Baryon Oscillation Spectroscopic Survey: Precision measurement of the absolute cosmic distance scale," in *astro2010: The Astronomy and Astrophysics Decadal Survey*, vol. 2010 of *ArXiv Astrophysics e-prints*, p. 314, 2009.

[2] D. J. Eisenstein, D. H. Weinberg, E. Agol, H. Aihara, C. Allende Prieto, S. F. Anderson, J. A. Arns, É. Aubourg, S. Bailey, E. Balbinot, and et al., "SDSS-III: Massive Spectroscopic Surveys of the Distant Universe, the Milky Way, and Extra-Solar Planetary Systems," AJ, vol. 142, p. 72, Sept. 2011.

[3] K. S. Dawson, D. J. Schlegel, C. P. Ahn, S. F. Anderson, É. Aubourg, S. Bailey, R. H. Barkhouser, J. E. Bautista, A. Beifiori, A. A. Berlind, V. Bhardwaj, D. Bizyaev, C. H. Blake, M. R. Blanton, M. Blomqvist, A. S. Bolton, A. Borde, J. Bovy, W. N. Brandt, H. Brewington, J. Brinkmann, P. J. Brown, J. R. Brownstein, K. Bundy, N. G. Busca, W. Carithers, A. R. Carnero, M. A. Carr, Y. Chen, J. Comparat, N. Connolly, F. Cope, R. A. C. Croft, A. J. Cuesta, L. N. da Costa, J. R. A. Davenport, T. Delubac, R. de Putter, S. Dhital, A. Ealet, G. L. Ebelke, D. J. Eisenstein, S. Escoffier, X. Fan, N. Filiz Ak, H. Finley, A. Font-Ribera, R. Génova-Santos, J. E. Gunn, H. Guo, D. Haggard, P. B. Hall, J.-C. Hamilton, B. Harris, D. W. Harris, S. Ho, D. W. Hogg, D. Holder, K. Honscheid, J. Huehnerhoff, B. Jordan, W. P. Jordan, G. Kauffmann, E. A. Kazin, D. Kirkby, M. A. Klaene, J.-P. Kneib, J.-M. Le Goff, K.-G. Lee, D. C. Long, C. P. Loomis, B. Lundgren, R. H. Lupton, M. A. G. Maia, M. Makler, E. Malanushenko, V. Malanushenko, R. Mandelbaum, M. Manera, C. Maraston, D. Margala, K. L. Masters, C. K. McBride, P. McDonald, I. D. McGreer, R. G. McMahon, O. Mena, J. Miralda-Escudé, A. D. Montero-Dorta, F. Montesano, D. Muna, A. D. Myers, T. Naugle, R. C. Nichol, P. Noterdaeme, S. E. Nuza, M. D. Olmstead, A. Oravetz, D. J. Oravetz, R. Owen, N. Padmanabhan, N. Palanque-Delabrouille, K. Pan, J. K. Parejko, I. Pâris, W. J. Percival, I. Pérez-Fournon, I. Pérez-Ràfols, P. Petitjean, R. Pfaffenberger, J. Pforr, M. M. Pieri, F. Prada, A. M. Price-Whelan, M. J. Raddick, R. Rebolo, J. Rich, G. T. Richards, C. M. Rockosi, N. A. Roe, A. J. Ross, N. P. Ross, G. Rossi, J. A. Rubiño-Martin, L. Samushia, A. G. Sánchez, C. Sayres, S. J. Schmidt, D. P. Schneider, C. G. Scóccola, H.-J. Seo, A. Shelden, E. Sheldon, Y. Shen, Y. Shu, A. Slosar, S. A. Smee, S. A. Snedden, F. Stauffer, O. Steele, M. A. Strauss, A. Streblyanska, N. Suzuki, M. E. C. Swanson, T. Tal, M. Tanaka, D. Thomas, J. L. Tinker, R. Tojeiro, C. A. Tremonti, M. Vargas Magaña, L. Verde, M. Viel, D. A. Wake, M. Watson, B. A. Weaver, D. H. Weinberg, B. J. Weiner, A. A. West, M. White, W. M. Wood-Vasey, C. Yeche, I. Zehavi, G.-B. Zhao, and Z. Zheng, "The Baryon Oscillation Spectroscopic Survey of SDSS-III," AJ, vol. 145, p. 10, Jan. 2013.

[4] A. G. Riess, A. V. Filippenko, P. Challis, A. Clocchiatti, A. Diercks, P. M. Garnavich, R. L. Gilliland, C. J. Hogan, S. Jha, R. P. Kirshner, B. Leibundgut, M. M. Phillips, D. Reiss, B. P. Schmidt, R. A. Schommer, R. C. Smith, J. Spyromilio, C. Stubbs, N. B. Suntzeff, and J. Tonry, "Observational Evidence from Supernovae for an Accelerating Universe and a Cosmological Constant," AJ, vol. 116, pp. 1009–1038, Sept. 1998.

[5] S. Perlmutter, G. Aldering, G. Goldhaber, R. A. Knop, P. Nugent, P. G. Castro, S. Deustua, S. Fabbro, A. Goobar, D. E. Groom, I. M. Hook, A. G. Kim, M. Y. Kim, J. C. Lee, N. J. Nunes, R. Pain, C. R. Pennypacker, R. Quimby, C. Lidman, R. S. Ellis, M. Irwin, R. G. McMahon, P. Ruiz-Lapuente, N. Walton, B. Schaefer, B. J. Boyle, A. V. Filippenko, T. Matheson, A. S. Fruchter, N. Panagia, H. J. M. Newberg, W. J. Couch, and T. S. C. Project, "Measurements of Ω and Λ from 42 High-Redshift Supernovae," ApJ, vol. 517, pp. 565–586, June 1999.

[6] D. H. Weinberg, M. J. Mortonson, D. J. Eisenstein, C. Hirata, A. G. Riess, and E. Rozo, "Observational probes of cosmic acceleration," Phys. Rep., vol. 530, pp. 87–255, Sept. 2013.

[7] D. J. Eisenstein, I. Zehavi, D. W. Hogg, R. Scoccimarro, M. R. Blanton, R. C. Nichol, R. Scranton, H.-J. Seo, M. Tegmark, Z. Zheng, S. F. Anderson, J. Annis, N. Bahcall, J. Brinkmann, S. Burles, F. J. Castander, A. Connolly, I. Csabai, M. Doi, M. Fukugita, J. A.

Frieman, K. Glazebrook, J. E. Gunn, J. S. Hendry, G. Hennessy, Z. Ivezić, S. Kent, G. R. Knapp, H. Lin, Y.-S. Loh, R. H. Lupton, B. Margon, T. A. McKay, A. Meiksin, J. A. Munn, A. Pope, M. W. Richmond, D. Schlegel, D. P. Schneider, K. Shimasaku, C. Stoughton, M. A. Strauss, M. SubbaRao, A. S. Szalay, I. Szapudi, D. L. Tucker, B. Yanny, and D. G. York, "Detection of the Baryon Acoustic Peak in the Large-Scale Correlation Function of SDSS Luminous Red Galaxies," ApJ, vol. 633, pp. 560–574, Nov. 2005.

[8] S. Cole, W. J. Percival, J. A. Peacock, P. Norberg, C. M. Baugh, C. S. Frenk, I. Baldry, J. Bland-Hawthorn, T. Bridges, R. Cannon, M. Colless, C. Collins, W. Couch, N. J. G. Cross, G. Dalton, V. R. Eke, R. De Propris, S. P. Driver, G. Efstathiou, R. S. Ellis, K. Glazebrook, C. Jackson, A. Jenkins, O. Lahav, I. Lewis, S. Lumsden, S. Maddox, D. Madgwick, B. A. Peterson, W. Sutherland, and K. Taylor, "The 2dF Galaxy Redshift Survey: power-spectrum analysis of the final data set and cosmological implications," MNRAS, vol. 362, pp. 505–534, Sept. 2005.

[9] Planck Collaboration, P. A. R. Ade, N. Aghanim, M. Arnaud, M. Ashdown, J. Aumont, C. Baccigalupi, A. J. Banday, R. B. Barreiro, J. G. Bartlett, and et al., "Planck 2015 results. XIII. Cosmological parameters," *ArXiv e-prints*, Feb. 2015.

[10] R. Jimenez and A. Loeb, "Constraining Cosmological Parameters Based on Relative Galaxy Ages," ApJ, vol. 573, pp. 37–42, July 2002.

[11] M. Moresco *et al.*, "Improved constraints on the expansion rate of the Universe up to z ˜ 1.1 from the spectroscopic evolution of cosmic chronometers," JCAP, vol. 8, p. 6, Aug. 2012.

[12] J. Simon, L. Verde, and R. Jimenez, "Constraints on the redshift dependence of the dark energy potential," Phys. Rev. D, vol. 71, p. 123001, June 2005.

[13] D. Stern, R. Jimenez, L. Verde, M. Kamionkowski, and S. A. Stanford, "Cosmic chronometers: constraining the equation of state of dark energy. I: H(z) measurements," JCAP, vol. 2, p. 8, Feb. 2010.

[14] M. Moresco, L. Verde, L. Pozzetti, R. Jimenez, and A. Cimatti, "New constraints on cosmological parameters and neutrino properties using the expansion rate of the Universe to z ˜ 1.75," JCAP, vol. 7, p. 53, July 2012.

[15] G.-B. Zhao, R. G. Crittenden, L. Pogosian, and X. Zhang, "Examining the Evidence for Dynamical Dark Energy," *Physical Review Letters*, vol. 109, p. 171301, Oct. 2012.

[16] X. Wang *et al.*, "Observational constraints on cosmic neutrinos and dark energy revisited," JCAP, vol. 11, p. 18, Nov. 2012.

[17] S. Riemer-Sørensen, D. Parkinson, T. M. Davis, and C. Blake, "Simultaneous Constraints on the Number and Mass of Relativistic Species," ApJ, vol. 763, p. 89, Feb. 2013.

[18] C. Maraston, J. Pforr, B. M. Henriques, D. Thomas, D. Wake, J. R. Brownstein, D. Capozzi, J. Tinker, K. Bundy, R. A. Skibba, A. Beifiori, R. C. Nichol, E. Edmondson, D. P. Schneider, Y. Chen, K. L. Masters, O. Steele, A. S. Bolton, D. G. York, B. A. Weaver, T. Higgs, D. Bizyaev, H. Brewington, E. Malanushenko, V. Malanushenko, S. Snedden, D. Oravetz, K. Pan, A. Shelden, and A. Simmons, "Stellar masses of SDSS-III/BOSS galaxies at $z \sim 0.5$ and constraints to galaxy formation models," MNRAS, vol. 435, pp. 2764–2792, Nov. 2013.

[19] A. G. Riess, L.-G. Strolger, S. Casertano, H. C. Ferguson, B. Mobasher, B. Gold, P. J. Challis, A. V. Filippenko, S. Jha, W. Li, J. Tonry, R. Foley, R. P. Kirshner, M. Dickinson, E. MacDonald, D. Eisenstein, M. Livio, J. Younger, C. Xu, T. Dahlén, and D. Stern, "New Hubble Space Telescope Discoveries of Type Ia Supernovae at z ≥1: Narrowing Constraints on the Early Behavior of Dark Energy," ApJ, vol. 659, pp. 98–121, Apr. 2007.

[20] J. A. S. Lima, J. F. Jesus, R. C. Santos, and M. S. S. Gill, "Is the transition redshift a new cosmological number?," *ArXiv e-prints*, May 2012.

[21] S. Capozziello, O. Farooq, O. Luongo, and B. Ratra, "Cosmographic bounds on the cosmological deceleration-acceleration transition redshift in f(R) gravity," Phys. Rev. D, vol. 90, p. 044016, Aug. 2014.

[22] S. Capozziello, O. Luongo, and E. N. Saridakis, "Transition redshift in f (T) cosmology and observational constraints," Phys. Rev. D, vol. 91, p. 124037, June 2015.

[23] T. Treu, R. S. Ellis, T. X. Liao, P. G. van Dokkum, P. Tozzi, A. Coil, J. Newman, M. C. Cooper, and M. Davis, "The Assembly History of Field Spheroidals: Evolution of Mass-to-Light Ratios and Signatures of Recent Star Formation," ApJ, vol. 633, pp. 174–197, Nov. 2005.

[24] A. Renzini, "Stellar Population Diagnostics of Elliptical Galaxy Formation," ARA&A, vol. 44, pp. 141–192, Sept. 2006.

[25] D. Thomas, C. Maraston, R. Bender, and C. Mendes de Oliveira, "The Epochs of Early-Type Galaxy Formation as a Function of Environment," ApJ, vol. 621, pp. 673–694, Mar. 2005.

[26] D. Thomas, C. Maraston, K. Schawinski, M. Sarzi, and J. Silk, "Environment and self-regulation in galaxy formation," MNRAS, vol. 404, pp. 1775–1789, June 2010.

[27] L. Pozzetti, M. Bolzonella, E. Zucca, G. Zamorani, S. Lilly, A. Renzini, M. Moresco, M. Mignoli, P. Cassata, L. Tasca, F. Lamareille, C. Maier, B. Meneux, C. Halliday, P. Oesch, D. Vergani, K. Caputi, K. Kovač, A. Cimatti, O. Cucciati, A. Iovino, Y. Peng, M. Carollo, T. Contini, J.-P. Kneib, O. Le Févre, V. Mainieri, M. Scodeggio, S. Bardelli, A. Bongiorno, G. Coppa, S. de la Torre, L. de Ravel, P. Franzetti, B. Garilli, P. Kampczyk, C. Knobel, J.-F. Le Borgne, V. Le Brun, R. Pellò, E. Perez Montero, E. Ricciardelli, J. D. Silverman, M. Tanaka, L. Tresse, U. Abbas, D. Bottini, A. Cappi, L. Guzzo, A. M. Koekemoer, A. Leauthaud, D. Maccagni, C. Marinoni, H. J. McCracken, P. Memeo, C. Porciani, R. Scaramella, C. Scarlata, and N. Scoville, "zCOSMOS - 10k-bright spectroscopic sample. The bimodality in the galaxy stellar mass function: exploring its evolution with redshift," A&A, vol. 523, p. A13, Nov. 2010.

[28] C. Conroy, G. J. Graves, and P. G. van Dokkum, "Early-type Galaxy Archeology: Ages, Abundance Ratios, and Effective Temperatures from Full-spectrum Fitting," ApJ, vol. 780, p. 33, Jan. 2014.

[29] R. M. McDermid, K. Alatalo, L. Blitz, F. Bournaud, M. Bureau, M. Cappellari, A. F. Crocker, R. L. Davies, T. A. Davis, P. T. de Zeeuw, P.-A. Duc, E. Emsellem, S. Khochfar, D. Krajnović, H. Kuntschner, R. Morganti, T. Naab, T. Oosterloo, M. Sarzi, N. Scott, P. Serra, A.-M. Weijmans, and L. M. Young, "The ATLAS^{3D} Project - XXX. Star formation histories and stellar population scaling relations of early-type galaxies," MNRAS, vol. 448, pp. 3484–3513, Apr. 2015.

[30] R. Bender, R. P. Saglia, B. Ziegler, P. Belloni, L. Greggio, U. Hopp, and G. Bruzual, "Exploring Cluster Elliptical Galaxies as Cosmological Standard Rods," ApJ, vol. 493, pp. 529–535, Jan. 1998.

[31] D. P. Carson and R. C. Nichol, "The age-redshift relation for luminous red galaxies in the Sloan Digital Sky Survey," MNRAS, vol. 408, pp. 213–233, Oct. 2010.

[32] M. Moresco, R. Jimenez, A. Cimatti, and L. Pozzetti, "Constraining the expansion rate of the Universe using low-redshift ellipticals as cosmic chronometers," JCAP, vol. 3, p. 45, Mar. 2011.

[33] G. Liu, Y. Lu, L. Xie, X. Chen, and Y. Zhao, "Quiescent Luminous Red Galaxies (LRGs) as Cosmic Chronometers: on the Significance of the Mass and Environmental Dependence," *ArXiv e-prints*, Sept. 2015.

[34] M. Franx and P. G. van Dokkum, "Measuring the Evolution of the M%TL ratio from the Fundamental Plane in CL 0024+16 at Z =0.39," in *New Light on Galaxy Evolution* (R. Bender and R. L. Davies, eds.), vol. 171 of *IAU Symposium*, p. 233, 1996.

[35] P. G. van Dokkum, M. Franx, D. Fabricant, G. D. Illingworth, and D. D. Kelson, "Hubble Space Telescope Photometry and Keck Spectroscopy of the Rich Cluster MS 1054-03: Morphologies, Butcher-Oemler Effect, and the Color-Magnitude Relation at Z = 0.83," ApJ, vol. 541, pp. 95–111, Sept. 2000.

[36] M. Moresco, L. Pozzetti, A. Cimatti, G. Zamorani, M. Bolzonella, F. Lamareille, M. Mignoli, E. Zucca, S. J. Lilly, C. M. Carollo, T. Contini, J.-P. Kneib, O. Le Fèvre, V. Mainieri, A. Renzini, M. Scodeggio, S. Bardelli, A. Bongiorno, K. Caputi, O. Cucciati, S. de la Torre, L. de Ravel, P. Franzetti, B. Garilli, A. Iovino, P. Kampczyk, C. Knobel, K. Kovač, J.-F. Le Borgne, V. Le Brun, C. Maier, R. Pelló, Y. Peng, E. Perez-Montero, V. Presotto, J. D. Silverman, M. Tanaka, L. Tasca, L. Tresse, D. Vergani, L. Barnes, R. Bordoloi, A. Cappi, C. Diener, A. M. Koekemoer, E. Le Floc'h, C. López-Sanjuan, H. J. McCracken, P. Nair, P. Oesch, C. Scarlata, N. Scoville, and N. Welikala, "Spot the difference. Impact of different selection criteria on observed properties of passive galaxies in zCOSMOS-20k sample," A&A, vol. 558, p. A61, Oct. 2013.

[37] A. G. Bruzual, "Spectral evolution of galaxies. I - Early-type systems," ApJ, vol. 273, pp. 105–127, Oct. 1983.

[38] D. Hamilton, "The spectral evolution of galaxies. I - an observational approach," ApJ, vol. 297, pp. 371–389, Oct. 1985.

[39] M. L. Balogh, S. L. Morris, H. K. C. Yee, R. G. Carlberg, and E. Ellingson, "Differential Galaxy Evolution in Cluster and Field Galaxies at z˜0.3," ApJ, vol. 527, pp. 54–79, Dec. 1999.

[40] M. White, M. Blanton, A. Bolton, D. Schlegel, J. Tinker, A. Berlind, L. da Costa, E. Kazin, Y.-T. Lin, M. Maia, C. K. McBride, N. Padmanabhan, J. Parejko, W. Percival, F. Prada, B. Ramos, E. Sheldon, F. de Simoni, R. Skibba, D. Thomas, D. Wake, I. Zehavi, Z. Zheng, R. Nichol, D. P. Schneider, M. A. Strauss, B. A. Weaver, and D. H. Weinberg, "The Clustering of Massive Galaxies at z ˜ 0.5 from the First Semester of BOSS Data," ApJ, vol. 728, p. 126, Feb. 2011.

[41] D. Thomas, O. Steele, C. Maraston, J. Johansson, A. Beifiori, J. Pforr, G. Strömbäck, C. A. Tremonti, D. Wake, D. Bizyaev, A. Bolton, H. Brewington, J. R. Brownstein, J. Comparat, J.-P. Kneib, E. Malanushenko, V. Malanushenko, D. Oravetz, K. Pan, J. K. Parejko, D. P. Schneider, A. Shelden, A. Simmons, S. Snedden, M. Tanaka, B. A. Weaver, and R. Yan, "Stellar velocity dispersions and emission line properties of SDSS-III/BOSS galaxies," MNRAS, vol. 431, pp. 1383–1397, May 2013.

[42] K. L. Masters, C. Maraston, R. C. Nichol, D. Thomas, A. Beifiori, K. Bundy, E. M. Edmondson, T. D. Higgs, A. Leauthaud, R. Mandelbaum, J. Pforr, A. J. Ross, N. P. Ross, D. P. Schneider, R. Skibba, J. Tinker, R. Tojeiro, D. A. Wake, J. Brinkmann, and B. A. Weaver, "The morphology of galaxies in the Baryon Oscillation Spectroscopic Survey," MNRAS, vol. 418, pp. 1055–1070, Dec. 2011.

[43] A. Citro, L. Pozzetti, M. Moresco, and A. Cimatti, "Inferring the star formation histories of the most massive and passive early-type galaxies at z>0.3," *arXiv:1604.07826*, Apr. 2016.

[44] C. Maraston and G. Strömbäck, "Stellar population models at high spectral resolution," MNRAS, vol. 418, pp. 2785–2811, Dec. 2011.

[45] R. Cid Fernandes, A. Mateus, L. Sodré, G. Stasińska, and J. M. Gomes, "Semi-empirical analysis of Sloan Digital Sky Survey galaxies - I. Spectral synthesis method," MNRAS, vol. 358, pp. 363–378, Apr. 2005.

[46] R. Tojeiro, A. F. Heavens, R. Jimenez, and B. Panter, "Recovering galaxy star formation and metallicity histories from spectra using VESPA," MNRAS, vol. 381, pp. 1252–1266, Nov. 2007.

[47] D. M. Wilkinson, C. Maraston, D. Thomas, L. Coccato, R. Tojeiro, M. Cappellari, F. Belfiore, M. Bershady, M. Blanton, K. Bundy, S. Cales, B. Cherinka, N. Drory, E. Emsellem, H. Fu,

D. Law, C. Li, R. Maiolino, K. Masters, C. Tremonti, D. Wake, E. Wang, A.-M. Weijmans, T. Xiao, R. Yan, K. Zhang, D. Bizyaev, J. Brinkmann, K. Kinemuchi, E. Malanushenko, V. Malanushenko, D. Oravetz, K. Pan, and A. Simmons, "P-MaNGA: full spectral fitting and stellar population maps from prototype observations," MNRAS, vol. 449, pp. 328–360, May 2015.

[48] G. Bruzual and S. Charlot, "Stellar population synthesis at the resolution of 2003," MNRAS, vol. 344, pp. 1000–1028, Oct. 2003.

[49] C. Maraston, E. Daddi, A. Renzini, A. Cimatti, M. Dickinson, C. Papovich, A. Pasquali, and N. Pirzkal, "Evidence for TP-AGB Stars in High-Redshift Galaxies, and Their Effect on Deriving Stellar Population Parameters," ApJ, vol. 652, pp. 85–96, Nov. 2006.

[50] J. Falcón-Barroso, P. Sánchez-Blázquez, A. Vazdekis, E. Ricciardelli, N. Cardiel, A. J. Cenarro, J. Gorgas, and R. F. Peletier, "An updated MILES stellar library and stellar population models," A&A, vol. 532, p. A95, Aug. 2011.

[51] J.-F. Le Borgne, G. Bruzual, R. Pelló, A. Lançon, B. Rocca-Volmerange, B. Sanahuja, D. Schaerer, C. Soubiran, and R. Vílchez-Gómez, "STELIB: A library of stellar spectra at R ˜ 2000," A&A, vol. 402, pp. 433–442, May 2003.

[52] A. Beifiori, C. Maraston, D. Thomas, and J. Johansson, "On the spectral resolution of the MILES stellar library," A&A, vol. 531, p. A109, July 2011.

[53] S. A. Smee, J. E. Gunn, A. Uomoto, N. Roe, D. Schlegel, C. M. Rockosi, M. A. Carr, F. Leger, K. S. Dawson, M. D. Olmstead, J. Brinkmann, R. Owen, R. H. Barkhouser, K. Honscheid, P. Harding, D. Long, R. H. Lupton, C. Loomis, L. Anderson, J. Annis, M. Bernardi, V. Bhardwaj, D. Bizyaev, A. S. Bolton, H. Brewington, J. W. Briggs, S. Burles, J. G. Burns, F. J. Castander, A. Connolly, J. R. A. Davenport, G. Ebelke, H. Epps, P. D. Feldman, S. D. Friedman, J. Frieman, T. Heckman, C. L. Hull, G. R. Knapp, D. M. Lawrence, J. Loveday, E. J. Mannery, E. Malanushenko, V. Malanushenko, A. J. Merrelli, D. Muna, P. R. Newman, R. C. Nichol, D. Oravetz, K. Pan, A. C. Pope, P. G. Ricketts, A. Shelden, D. Sandford, W. Siegmund, A. Simmons, D. S. Smith, S. Snedden, D. P. Schneider, M. SubbaRao, C. Tremonti, P. Waddell, and D. G. York, "The Multi-object, Fiber-fed Spectrographs for the Sloan Digital Sky Survey and the Baryon Oscillation Spectroscopic Survey," AJ, vol. 146, p. 32, Aug. 2013.

[54] R. Cid Fernandes, Q. Gu, J. Melnick, E. Terlevich, R. Terlevich, D. Kunth, R. Rodrigues Lacerda, and B. Joguet, "The star formation history of Seyfert 2 nuclei," MNRAS, vol. 355, pp. 273–296, Nov. 2004.

[55] R. Tojeiro, S. Wilkins, A. F. Heavens, B. Panter, and R. Jimenez, "A Public Catalog of Stellar Masses, Star Formation and Metallicity Histories, and Dust Content from the Sloan Digital Sky Survey using VESPA," ApJS, vol. 185, pp. 1–19, Nov. 2009.

[56] S. Charlot and S. M. Fall, "A Simple Model for the Absorption of Starlight by Dust in Galaxies," ApJ, vol. 539, pp. 718–731, Aug. 2000.

[57] B. Panter, A. F. Heavens, and R. Jimenez, "Star formation and metallicity history of the SDSS galaxy survey: unlocking the fossil record," MNRAS, vol. 343, pp. 1145–1154, Aug. 2003.

[58] A. Gallazzi, S. Charlot, J. Brinchmann, S. D. M. White, and C. A. Tremonti, "The ages and metallicities of galaxies in the local universe," MNRAS, vol. 362, pp. 41–58, Sept. 2005.

[59] R. Jimenez, M. Bernardi, Z. Haiman, B. Panter, and A. F. Heavens, "The Ages, Metallicities, and Star Formation Histories of Early-Type Galaxies in the SDSS," ApJ, vol. 669, pp. 947–951, Nov. 2007.

[60] B. Panter, R. Jimenez, A. F. Heavens, and S. Charlot, "The cosmic evolution of metallicity from the SDSS fossil record," MNRAS, vol. 391, pp. 1117–1126, Dec. 2008.

[61] S. Toft, A. Gallazzi, A. Zirm, M. Wold, S. Zibetti, C. Grillo, and A. Man, "Deep Absorption Line Studies of Quiescent Galaxies at z ˜ 2: The Dynamical-mass-Size Relation and First Constraints on the Fundamental Plane," ApJ, vol. 754, p. 3, July 2012.

[62] M. Onodera, C. M. Carollo, A. Renzini, M. Cappellari, C. Mancini, N. Arimoto, E. Daddi, R. Gobat, V. Strazzullo, S. Tacchella, and Y. Yamada, "The Ages, Metallicities, and Element Abundance Ratios of Massive Quenched Galaxies at z = 1.6," ApJ, vol. 808, p. 161, Aug. 2015.

[63] D. C. Hoaglin, F. Mosteller, and J. W. Tukey, *Understanding robust and exploratory data anlysis*. 1983.

[64] A. Fontana, L. Pozzetti, I. Donnarumma, A. Renzini, A. Cimatti, G. Zamorani, N. Menci, E. Daddi, E. Giallongo, M. Mignoli, C. Perna, S. Salimbeni, P. Saracco, T. Broadhurst, S. Cristiani, S. D'Odorico, and R. Gilmozzi, "The K20 survey. VI. The distribution of the stellar masses in galaxies up to z $\simeq$ 2," A&A, vol. 424, pp. 23–42, Sept. 2004.

[65] A. Cimatti, "The Cosmic Evolution of Early-type Galaxies," in *IAU Symposium* (F. Combes and J. Palouš, eds.), vol. 235 of *IAU Symposium*, pp. 350–354, May 2007.

[66] A. Cimatti, "The formation and evolution of early-type galaxies: solid results and open questions," in *American Institute of Physics Conference Series* (G. Giobbi, A. Tornambe, G. Raimondo, M. Limongi, L. A. Antonelli, N. Menci, and E. Brocato, eds.), vol. 1111 of *American Institute of Physics Conference Series*, pp. 191–198, May 2009.

[67] C. Zhang, H. Zhang, S. Yuan, S. Liu, T.-J. Zhang, and Y.-C. Sun, "Four new observational H(z) data from luminous red galaxies in the Sloan Digital Sky Survey data release seven," *Research in Astronomy and Astrophysics*, vol. 14, pp. 1221–1233, Oct. 2014.

[68] M. Moresco, "Raising the bar: new constraints on the Hubble parameter with cosmic chronometers at $z \sim 2$," MNRAS, vol. 450, pp. L16–L20, June 2015.

[69] A. G. Riess, L. Macri, S. Casertano, H. Lampeitl, H. C. Ferguson, A. V. Filippenko, S. W. Jha, W. Li, and R. Chornock, "A 3% Solution: Determination of the Hubble Constant with the Hubble Space Telescope and Wide Field Camera 3," ApJ, vol. 730, p. 119, Apr. 2011.

[70] E. M. L. Humphreys, M. J. Reid, J. M. Moran, L. J. Greenhill, and A. L. Argon, "Toward a New Geometric Distance to the Active Galaxy NGC 4258. III. Final Results and the Hubble Constant," ApJ, vol. 775, p. 13, Sept. 2013.

[71] A. J. Cuesta, M. Vargas-Magaña, F. Beutler, A. S. Bolton, J. R. Brownstein, D. J. Eisenstein, H. Gil-Marín, S. Ho, C. K. McBride, C. Maraston, N. Padmanabhan, W. J. Percival, B. A. Reid, A. J. Ross, N. P. Ross, A. G. Sánchez, D. J. Schlegel, D. P. Schneider, D. Thomas, J. Tinker, R. Tojeiro, L. Verde, and M. White, "The clustering of galaxies in the SDSS-III Baryon Oscillation Spectroscopic Survey: Baryon Acoustic Oscillations in the correlation function of LOWZ and CMASS galaxies in Data Release 12," *ArXiv e-prints*, Sept. 2015.

[72] N. G. Busca *et al.*, "Baryon acoustic oscillations in the Lyα forest of BOSS quasars," A&A, vol. 552, p. A96, Apr. 2013.

[73] O. Farooq and B. Ratra, "Hubble Parameter Measurement Constraints on the Cosmological Deceleration-Acceleration Transition Redshift," ApJ, vol. 766, p. L7, Mar. 2013.

[74] O. Farooq, S. Crandall, and B. Ratra, "Binned Hubble parameter measurements and the cosmological deceleration-acceleration transition," *Physics Letters B*, vol. 726, pp. 72–82, Oct. 2013.

[75] N. Rani, D. Jain, S. Mahajan, A. Mukherjee, and N. Pires, "Transition redshift: new constraints from parametric and nonparametric methods," JCAP, vol. 12, p. 045, Dec. 2015.

[76] H. Akaike, "A New Look at the Statistical Model Identification," *IEEE Transactions on Automatic Control*, vol. 19, pp. 716–723, 1974.

[77] G. Schwarz, "Estimating the dimension of a model," *Ann. Statist*, vol. 6, pp. 461–464, 1978.

[78] A. R. Liddle, "Information criteria for astrophysical model selection," MNRAS, vol. 377, pp. L74–L78, May 2007.

[79] N. Sugiura, "Further analysis of the data by Akaikes information criterion and the finite corrections," *Communications in Statistics - Theory and Methods, A7, 13*, 1978.

[80] H. Jeffreys, *Theory of Probability*. 1961.

[81] R. Laureijs, J. Amiaux, S. Arduini, J. . Augueres, J. Brinchmann, R. Cole, M. Cropper, C. Dabin, L. Duvet, A. Ealet, and et al., "Euclid Definition Study Report," *ArXiv e-prints*, Oct. 2011.

[82] D. Spergel, N. Gehrels, J. Breckinridge, M. Donahue, A. Dressler, B. S. Gaudi, T. Greene, O. Guyon, C. Hirata, J. Kalirai, N. J. Kasdin, W. Moos, S. Perlmutter, M. Postman, B. Rauscher, J. Rhodes, Y. Wang, D. Weinberg, J. Centrella, W. Traub, C. Baltay, J. Colbert, D. Bennett, A. Kiessling, B. Macintosh, J. Merten, M. Mortonson, M. Penny, E. Rozo, D. Savransky, K. Stapelfeldt, Y. Zu, C. Baker, E. Cheng, D. Content, J. Dooley, M. Foote, R. Goullioud, K. Grady, C. Jackson, J. Kruk, M. Levine, M. Melton, C. Peddie, J. Ruffa, and S. Shaklan, "Wide-Field InfraRed Survey Telescope-Astrophysics Focused Telescope Assets WFIRST-AFTA Final Report," *ArXiv e-prints*, May 2013.

[83] M. Levi, C. Bebek, T. Beers, R. Blum, R. Cahn, D. Eisenstein, B. Flaugher, K. Honscheid, R. Kron, O. Lahav, P. McDonald, N. Roe, D. Schlegel, and representing the DESI collaboration, "The DESI Experiment, a whitepaper for Snowmass 2013," *ArXiv e-prints*, Aug. 2013.

[84] LSST Science Collaboration, P. A. Abell, J. Allison, S. F. Anderson, J. R. Andrew, J. R. P. Angel, L. Armus, D. Arnett, S. J. Asztalos, T. S. Axelrod, and et al., "LSST Science Book, Version 2.0," *ArXiv e-prints*, Dec. 2009.